



Perspectives on Titanium Science and Technology

Dipankar Banerjee ^{a,*}, J.C. Williams ^{b,c}

^a Department of Materials Engineering, Indian Institute of Science, Bangalore, India

^b Department of Materials Science and Engineering, University of North Texas, Denton, TX, USA

^c The Ohio State University, Columbus, OH, USA

Abstract

The basic framework and - conceptual understanding of the metallurgy of Ti alloys is strong and this has enabled the use of titanium and its alloys in safety-critical structures such as those in aircraft and aircraft engines. Nevertheless, a focus on cost-effectiveness and the compression of product development time by effectively integrating design with manufacturing in these applications, as well as those emerging in bioengineering, has driven research in recent decades towards a greater predictive capability through the use of computational materials engineering tools. Therefore this paper focuses on the complexity and variety of fundamental phenomena in this material system with a focus on phase transformations and mechanical behaviour in order to delineate the challenges that lie ahead in achieving these goals.

© 2012 Acta Materialia Inc. Published by Elsevier Ltd. All rights reserved.

Keywords: Titanium alloys; Phase transformations; Mechanical behaviour

1. Introduction

Recent compilations [1–3] provide exhaustive descriptions of the science, technology and application of titanium. Over the past 20 years, titanium and titanium alloy production practices have matured more rapidly than perhaps any structural material in the history of metallurgy. Fig. 1 provides examples of the growth in the use of titanium in widely differing applications, and with a range of engineering demands, that in many cases impact human safety and well-being. These highly successful applications have been largely guided by enlightened empiricism covering the practical aspects of Ti ingot melting and processing into mill products, and secondary fabrication. Still, significant variation in material performance requires including an appropriate degree of conservatism where design practices are concerned. The focus on eliminating production defects starting from extraction and melting

practice to machining and joining in order to improve the performance and reliability of titanium alloys and to avoid unexpected failures has been unusually high and has produced good results. We note that the major barrier to a still broader application range of Ti and Ti alloy continues to be cost. One large element of the cost of Ti is the necessity to reduce oxides or chlorides of Ti to the metallic form. The current industrial reduction process, devised long ago by Kroll, is energy-intensive and is a batch process. Currently, there are several efforts underway to use alternative reduction methods to produce either metallic Ti or alloyed Ti by co-reduction of mixed chlorides. Several of these methods have been shown to be feasible at the laboratory scale, but scale-up to production quantities is proving more challenging than originally thought.

However, significant gaps in physics-based models that capture the multitude of various phenomena that govern these engineering processes continue to exist even as models evolve. We have attempted to capture in this paper several aspects of the evolving science of titanium, related to its physical metallurgy. We believe that these developments

* Corresponding author. Tel.: +91 80 22932558.

E-mail address: dbanerjee@materials.iisc.ernet.in (D. Banerjee).

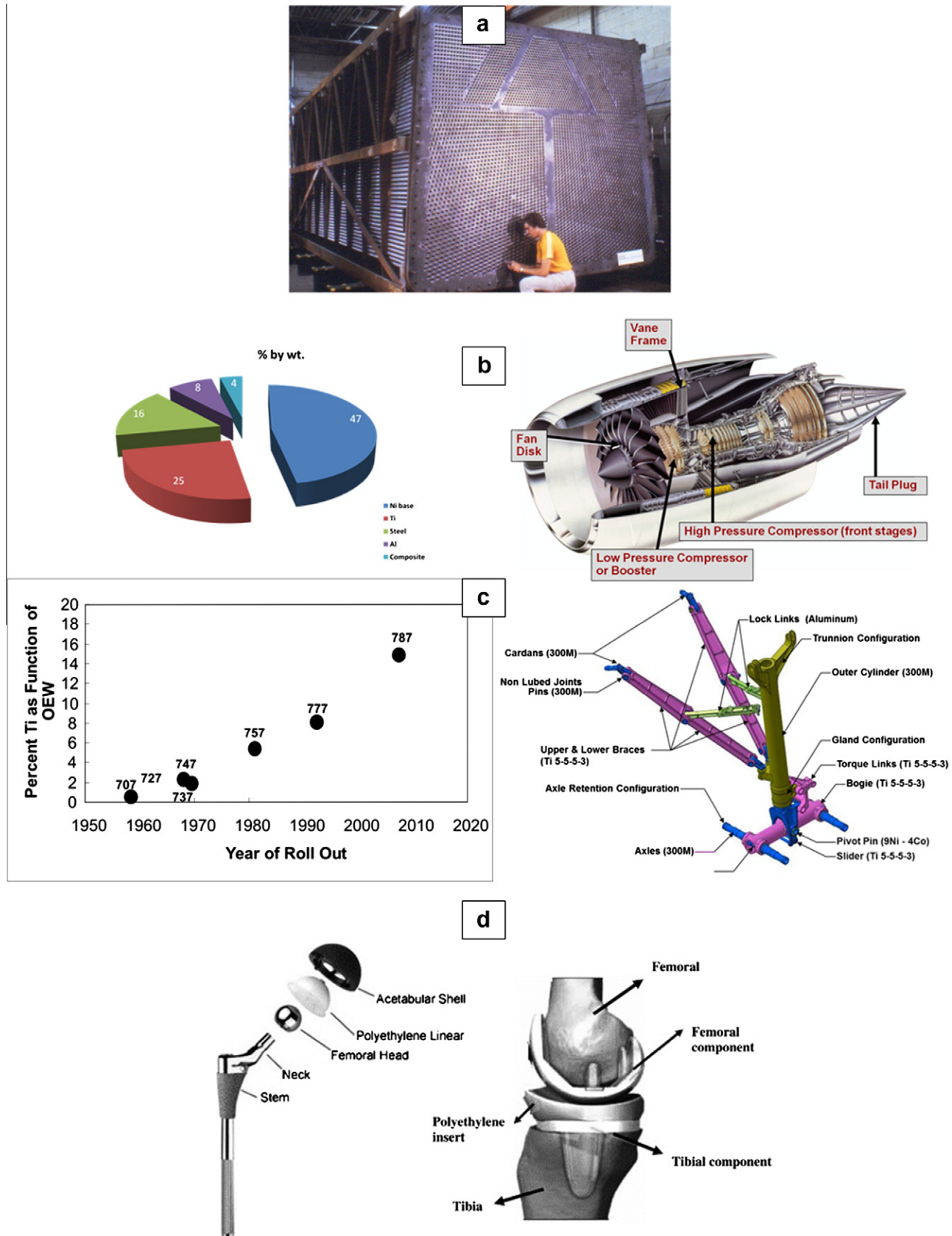


Fig. 1. Applications of titanium: (a) alpha titanium in tubing for heat exchangers (courtesy JA Hall), (b) near alpha and alpha + beta alloys in aeroengines [1], (c) high strength metastable beta alloys in airframes, as percentage of overall aircraft weight and in landing gear of the Boeing 787 [120], (d) a titanium hip replacement [73].

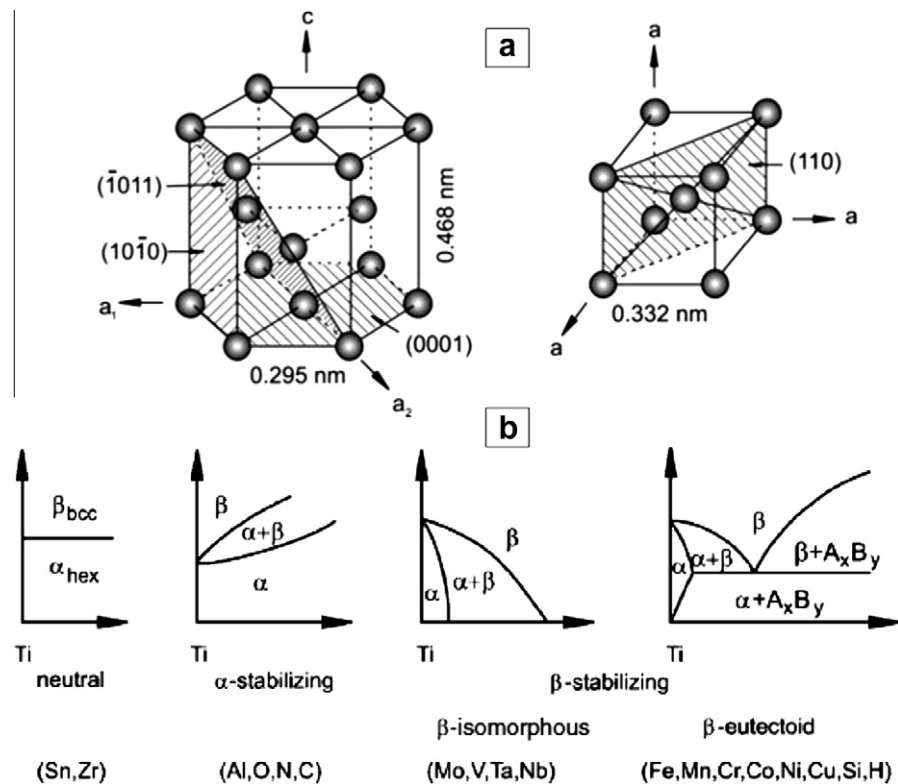


Fig. 2. (a) The hcp (alpha) and bcc (beta) structure of titanium. (b) Categories of titanium phase diagrams formed with different alloying additions.

will continue to challenge and inform efforts towards a greater computational and simulation capability supporting the processing–structure–property paradigm of this material system.

Titanium and its alloys derive many of their properties from the metal's allotropic modifications (Fig. 2a) at 1155 K from the low temperature hexagonal close packed (hcp) (alpha) phase to the high temperature, body centred cubic (bcc) (beta) phase. The ability to manipulate these properties is dependent on the effect of alloying on the stability and physical and mechanical behaviour of these two phases both individually and in a variety of microstructural permutations and combinations. Thus, single-phase alpha alloys are extensively used in applications that are not particularly demanding in terms of strength but focus more on the attractive corrosion resistance of titanium (Fig. 1a). Alternatively, two-phase alpha + beta alloys offer a range of combinations of strength, toughness and high temperature properties that make them attractive in wide ranging aerospace and other products demanding high specific properties to temperatures of ~ 873 K (Fig. 1b). The metallurgy of beta alloys enables the development of compositions and processing routes that can satisfy diverse requirements of very high strength with adequate toughness and fatigue resistance required in airframe applications (Fig. 1c) or meeting requirements of low modulus and biocompatibility with shape memory response and fatigue strength for use in biomedical applications (Fig. 1d).

2. Phase equilibria and phase transformations

Various classes of phase diagrams (Fig. 2b) may be used to illustrate the effect of alloying on titanium: those that show increasing alpha or beta stability with alloying addition or those in which alpha and beta stability remain neutral. Fig. 3 superimposes alpha and beta phase stability for common alloying additions. Within the beta stabilizer category, refractory metals such as Mo and W cause an immiscibility gap in the beta phase, leading to a monotectoid reaction, while the beta stabilizers Cr, Fe, Cu, Ni and Si form intermetallic compounds through a eutectoid reaction. The extensive solubility of oxygen and nitrogen in titanium also makes this metal unusual. These elements are extremely strong alpha stabilizers, creating the unusual situation where the lower temperature allotropic form, the alpha phase, can form directly from the liquid as an intermediate disordered phase, for example in a Ti-27 at.% O composition. As a consequence (and due to the absence of sulfur in raw materials), titanium alloys do not contain oxide, nitride or sulfide inclusions that commonly initiate failure in other structural metals. Hydrogen stabilizes the beta phase and falls into the category of eutectoid formers while carbon is another alpha stabilizer but has a much lower solubility in the alpha phase than oxygen or nitrogen. Boron has low solubility in both the alpha and beta phases, and is a departure from these common categories in that the alpha phase in the Ti-B system forms from a

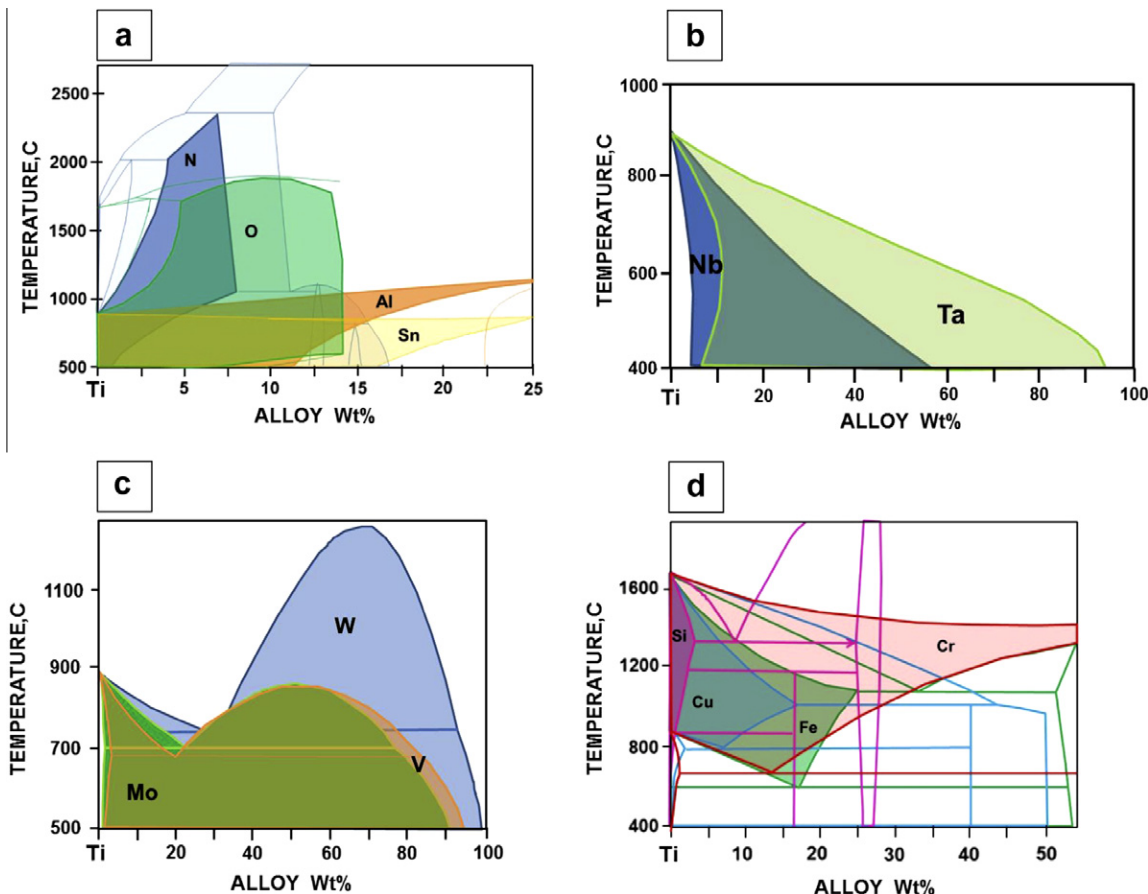


Fig. 3. The effect of various alloying additions on alpha and beta phase stability. The alpha and beta phases are shaded in each case to illustrate solubility and stability: (a) alpha stabilizers, (b) beta stabilizers with continuous solubility, (c) beta stabilizers with an immiscibility gap in the beta phase, (d) eutectoid systems with intermetallic compound formation.

peritectoid reaction between beta titanium and TiB. A thermodynamic database for titanium is now commercially available and is described by Saunders [4], but quantitative descriptions of phase equilibria in multicomponent commercial alloys and associated kinetics of transformations are rare.

The majority of engineering titanium alloys are based on the alpha or beta phases or a combination of the two in varying proportions in different alloys. Significant exceptions are alloys based on the intermetallics in the Ti-Al system or composites containing SiC fibre. We shall not include these or other titanium-based intermetallic compounds in our review.

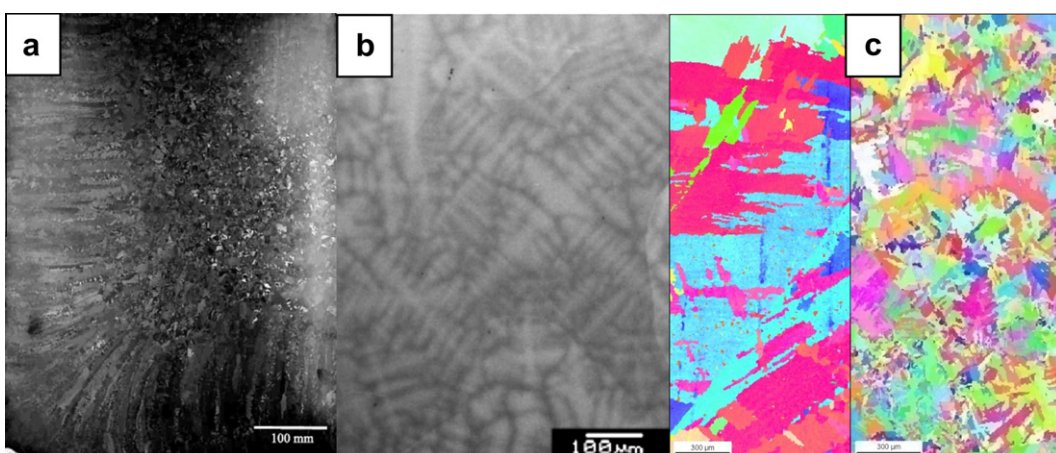


Fig. 4. (a) The macrostructure of vacuum arc remelted ingot [5]. (b) Microsegregation in a beta-rich alloy [121]. (c) The effect of boron (right) on reducing the as-cast grain size [122].

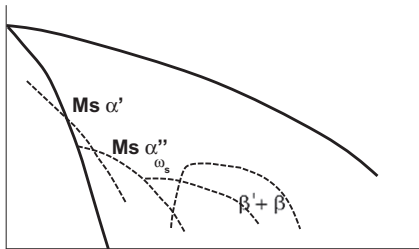


Fig. 5. A schematic beta isomorphous phase diagram showing various metastable reaction products and related phase fields.

2.1. Solidification

Titanium alloys, with the exceptions noted earlier, solidify into the beta phase. Due to the extreme reactivity of molten titanium, vacuum arc remelting, electron beam

or plasma cold hearth remelting or sometimes induction skull melting methods are employed to synthesize titanium alloys. The resulting ingot solidification structure can be columnar next to chill zones adjacent to water-cooled Cu crucibles with a $\langle 100 \rangle$ fibre texture along the $\langle 100 \rangle$ growth direction of the columnar grains, or equiaxed with a random texture [5,6]. Eutectoid elements such as iron are commonly used as beta stabilizing additions but also create a low melting eutectic. This can lead to solute segregation in larger ingots unless special precautions are employed. Microsegregation is observed with increasing beta stabilizer content and an examination of partitioning coefficients suggests that Nb and Mo are the species most likely to segregate. Improved solidification models would help define melt practices that would minimize these effects. Boron at very low levels is known to significantly refine as

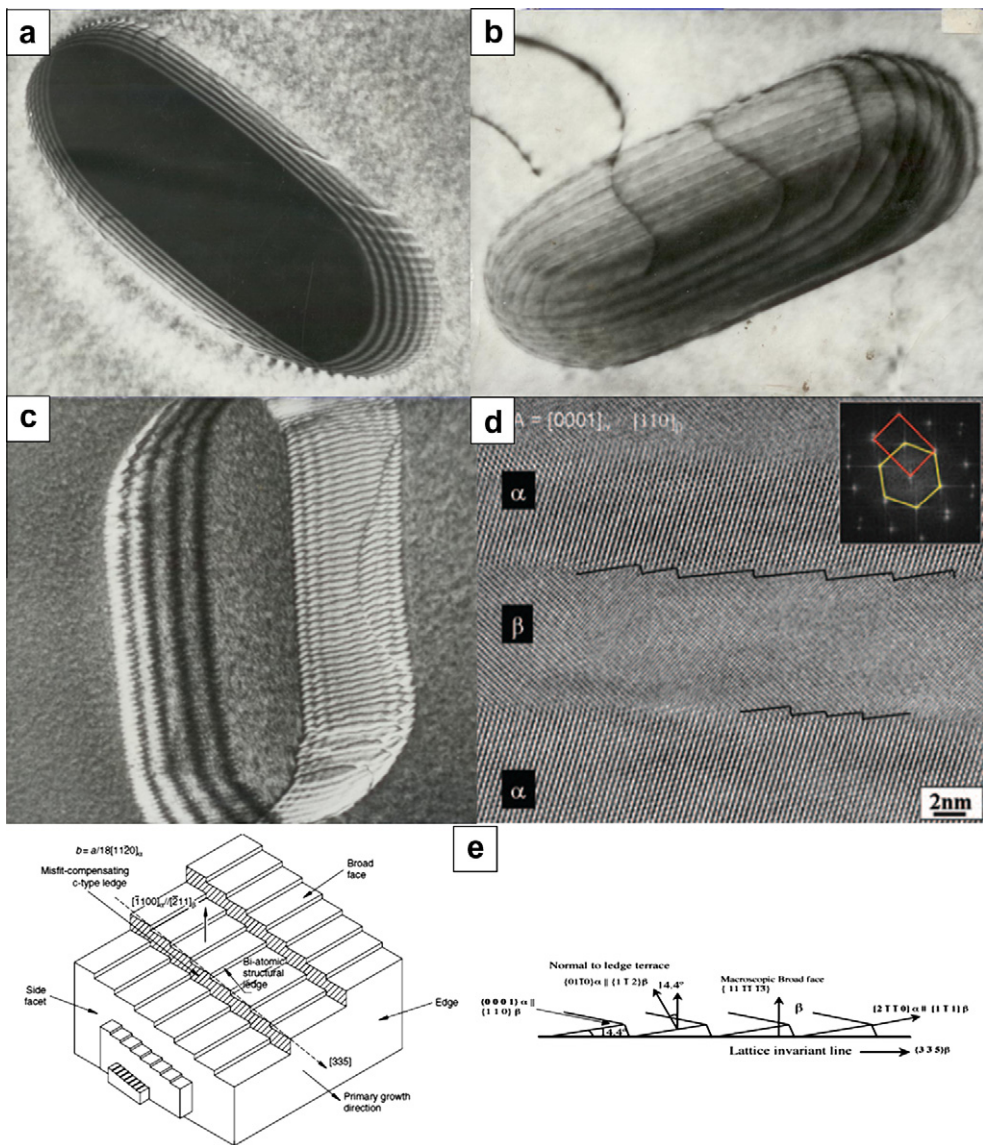


Fig. 6. The precipitation of alpha from the beta phase: (a) a coherent precipitate with growth ledges [123], (b) acquisition of misfit dislocations from the matrix [123], (c) a fully formed semicoherent interface structure [123], (d) a high resolution TEM image of the interface structure [124], (e) schematics of the geometry and crystallography of the interface structure (from Refs. [3,13]).

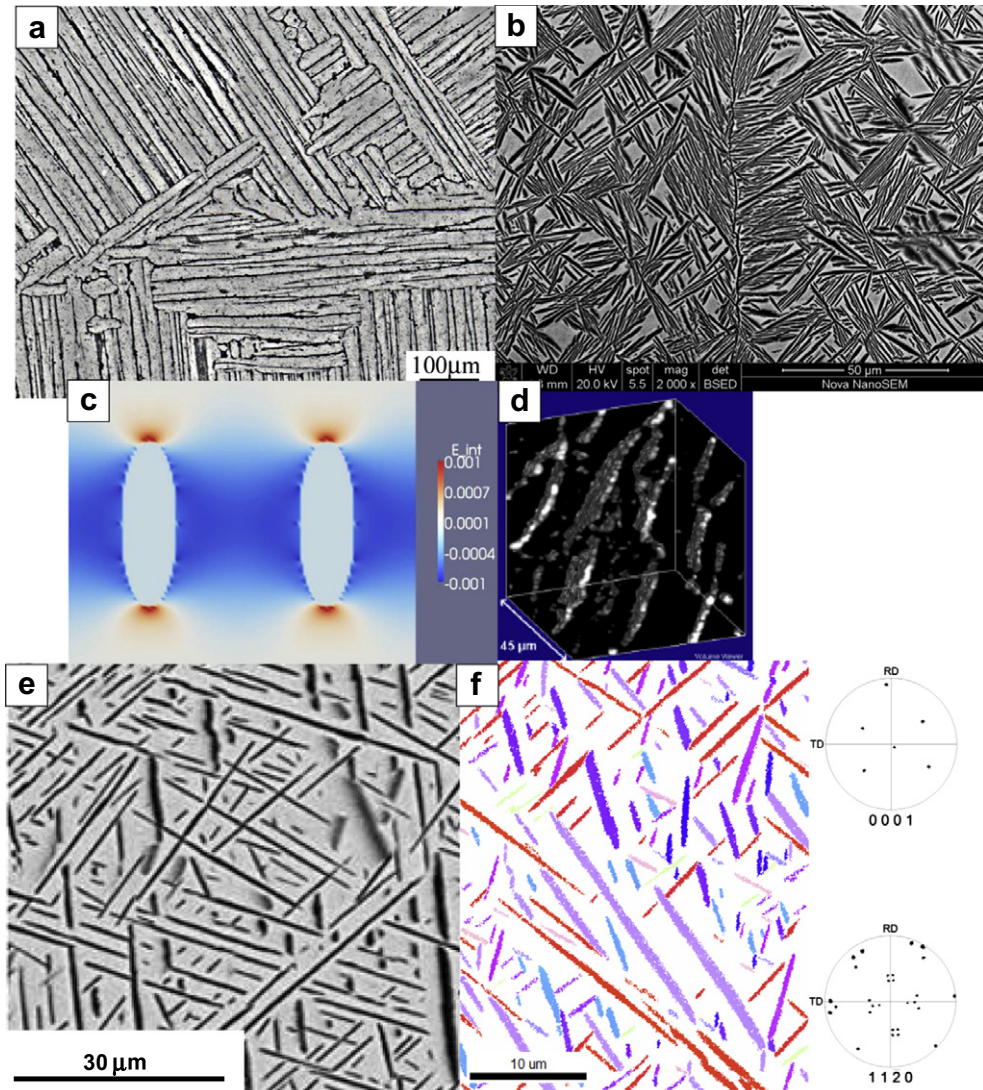


Fig. 7. The distribution of alpha: (a) in a near alpha alloy IMI834 cooled relatively slowly from above the beta transus (courtesy TK Nandy), (b) alpha variant distribution in Ti-3 at.% Mo showing bundles of intragranular alpha and a thin layer of grain boundary alpha at the centre of the micrograph and vertically oriented (courtesy D Choudhuri), (c) the interaction energy between parallel-oriented identical crystallographic variants from phase field simulations [9], (d) a 3-D image of beta films separating alpha laths in microstructures such as in (a) [16], (e) the distribution of alpha phase in the Ti-17 alloy, and (f) OIM of such variants and associated pole figures indicating the presence of all 12 variants of the alpha phase [125].

the solidified grain size [7] by mechanisms which are not well established but may be related to constitutional supercooling effects. Some of these effects are shown in Fig. 4.

2.2. Solid state phase transformations

A typical schematic phase diagram of titanium alloyed with increasing beta stabilizing content is shown in Fig. 5 and includes the metastable transformations to hexagonal or orthorhombic martensite, the omega phase and a phase separation reaction.

2.2.1. The equilibrium alpha phase

The morphology, orientation and distribution of the equilibrium alpha phase that forms from beta are of considerable significance. The defining characteristic of this transformation is the Burgers orientation relationship

(BOR) between the two phases: $\{110\}\beta/\langle0001\rangle\alpha$; $\langle\bar{1}\bar{1}\rangle\beta/\langle11\bar{2}0\rangle\alpha$. This orientation relationship results in 12 possible crystallographic variants of alpha in a single parent grain. The alpha phase forms as laths with broad faces that are semicoherent and contain structural ledges and dislocations [8], as shown in Fig. 6. Coherent alpha phase is rarely observed although the critical nucleus itself may be coherent. Fig. 6 shows an exception in the alloy Ti-0.3 Mo-0.8 Ni (TiCode12), and also illustrates the acquisition of interfacial misfit dislocations from the matrix by a coherent precipitate. Fig. 7 shows the variety of alpha variant distributions that can result from the beta-to-alpha transformation. In alloys lean in beta stabilizer content and at relatively slow cooling rates from the beta phase field, the alpha phase forms in colonies of laths, which are all the same variant of the BOR (Fig. 7a). On the other hand, basket-weave structures in which a more uniform

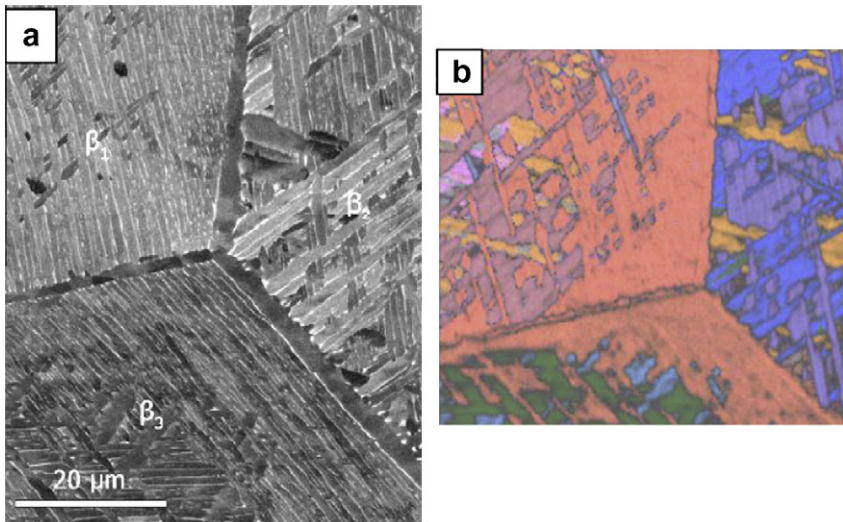


Fig. 8. Grain boundary alpha: (a) side plates from grain boundary α growing into β grains β_1 and β_3 , (b) the orientation image shows that the side plates have a common basal plane orientation with the grain boundary α at the boundaries between all three grains [35].

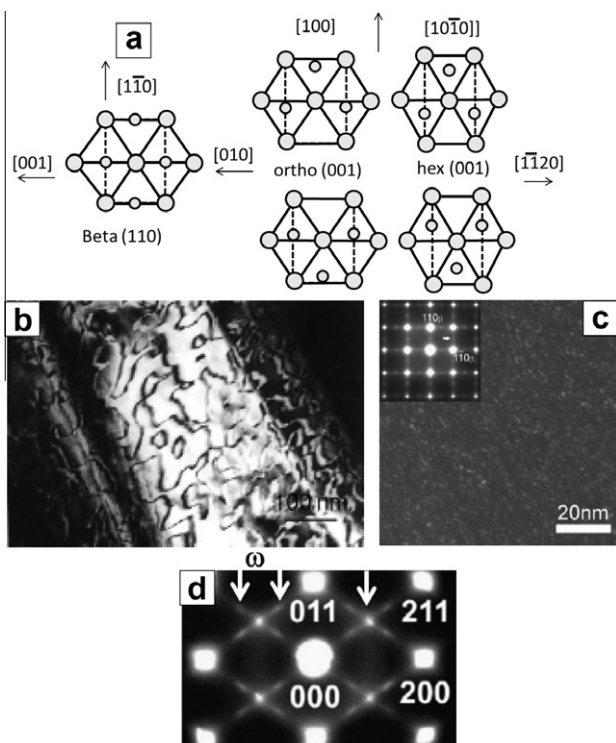


Fig. 9. The martensitic transformation. (a) The lattice correspondence describing the martensitic transformation from the parent beta to orthorhombic or hexagonal martensite in a projection perpendicular to $[1\bar{1}0]$ beta. The transformation is accomplished by the Bain distortion to either the orthorhombic or hexagonal symmetry as well as a shuffle on every alternate $(1\bar{1}0)$ plane in the $[1\bar{1}0]$ direction. (b) The shuffle can occur in opposite directions, as shown in (a), leading to the formation of domains within a hexagonal or orthorhombic martensite plate [19]. (c) The shuffle can also lead to the formation of nanodomains without a martensitic transformation [20]. (d) Omega reflections and maxima arising from $\langle 1\bar{1}0 \rangle$ relrods from an energy filtered diffraction pattern in a $[1\bar{1}0]$ beta zone axis [21]. Note that the rigid body rotation and lattice invariant shear of the martensite to realize an invariant plane is not shown in (a).

distribution of the 12 possible variants occurs appear at low transformation temperatures that result from fast cooling of alpha-rich alloys or isothermal heat treatment of beta-stabilizer-rich alloys (Fig. 7b and e). Several features of these transformation products remain poorly understood at this time. The origin of the colony structure has not been probed in any detail. It is possible that each colony forms as a consequence of side plates that emanate as a single variant of the BOR from alpha that forms first at the beta grain boundaries (see Fig. 8). However, the formation of groups of identical crystallographic variants persists, even when the nucleation process is clearly intra-granular (Fig. 7b). Preliminary phase field calculations show that a negative interaction energy does exist between two identical crystallographic variants oriented parallel to each other when elastic anisotropy of the alpha phase is included in the calculation (Fig. 7c) [9]. In alloys strongly enriched in beta stabilizers and when transformation occurs at low undercooling, triangular arrangements of individual variants dominate (Fig. 7e and f). Whether these arrangements are examples of self-accommodated variant distributions governed by elastic interactions [10,11] or whether these are a statistical consequence of random nucleation of the 12 crystallographic variants is not completely clear.

Alpha that nucleates and grows on beta grain boundaries (Fig. 8) also forms with the Burgers relationship with one of the grains on either side of the boundary [12], or with both grains in the case where the adjacent beta grains are specially related [13] (as we shall see later). Side plates emanate from the grain boundary alpha into the grain with which the BOR is satisfied. The microstructure can be dominated by these side plates when the transformation takes place at high temperatures when growth rates are high and nucleation rates low, for example during slow cooling of

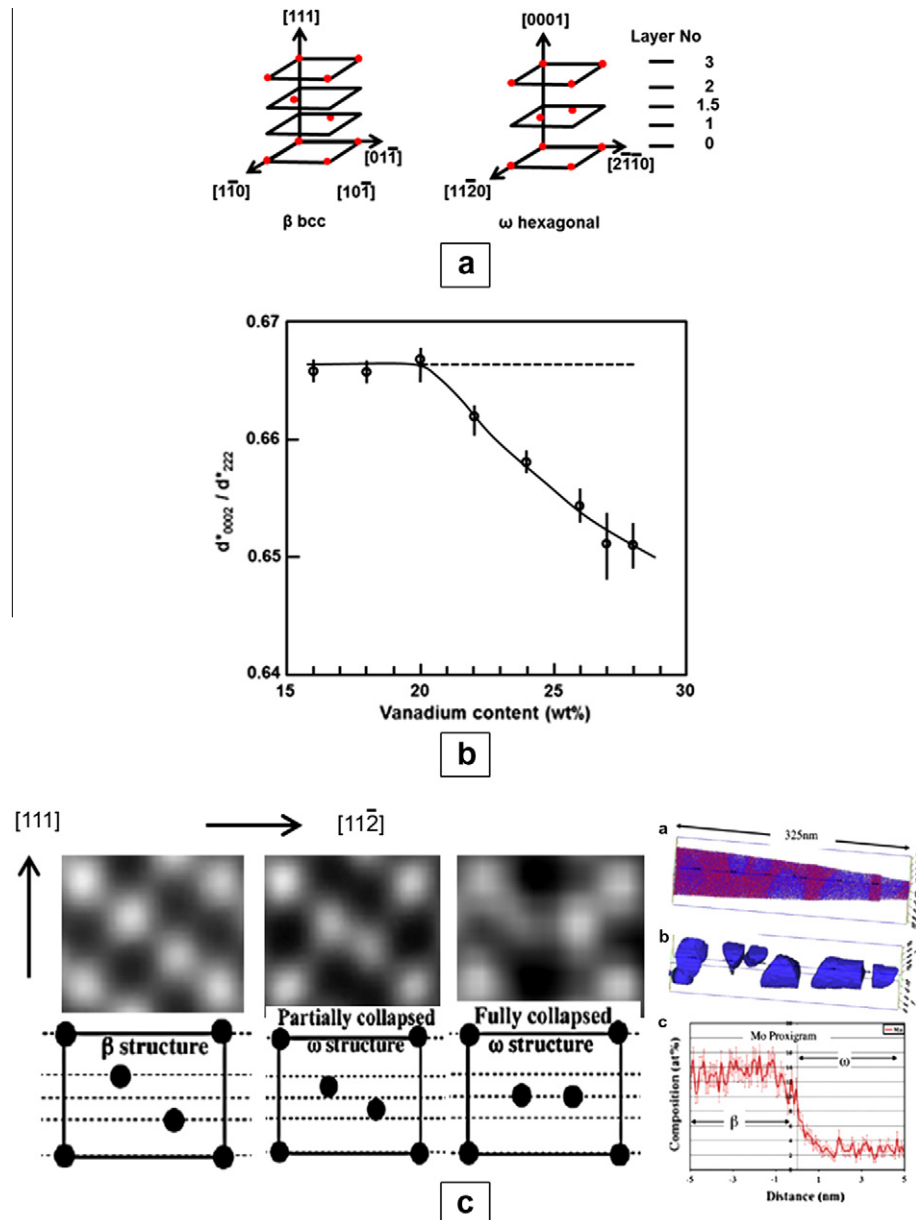


Fig. 10. (a) The atomic displacement in the beta-to-omega transformation [3]. (b) The variation of d^*_{0002}/d^*_{222} with V content in the Ti–V system [23]. (c) HAADF images showing beta phase, partially collapsed and fully collapsed (111) planes in the omega structure along with compositions of the beta and thermal omega phase determined by atom probe microanalysis of an isothermally aged sample of a Ti–9 at.% Mo alloy [29].

alpha-stabilizer-rich alloys. Since grain boundary alpha can form with the Burgers relationship with either neighbouring beta grain, a choice of 24 variants is available, of which one or two appear to dominate in a given grain boundary. If adjacent beta grain boundaries share a common {110} plane, the preferred variant always has its basal plane parallel to this common beta {110}. When this is not the case, it has been suggested [12] that the preferred variant will be that which has its close common close packed direction, $\langle 1\bar{1}1 \rangle\beta/\langle 11\bar{2}0 \rangle\alpha$, lying closest to the boundary plane. We have observed [9] examples of variants that do not satisfy the latter criterion, and conclude that grain boundary alpha variant selection mechanisms remain incompletely understood at this time, including whether the selection

process is nucleation dominated or growth dominated. In addition, the alpha phase can also be nucleated from omega [14]. An unusual isothermal transformation of the beta phase to an orthorhombic structure has also been recently reported [15]. The orthorhombic structure represents an intermediate state between beta and alpha and is usually observed as a martensite phase, discussed in greater detail below. Increasing efforts are being made to understand the three-dimensional (3-D) morphology and distribution of alpha laths and the remnant beta matrix (Fig. 7d) [16,17], because of the importance of a quantified understanding of these features.

The principal source of strength (as well as of strain incompatibility and stress inhomogeneity) in titanium

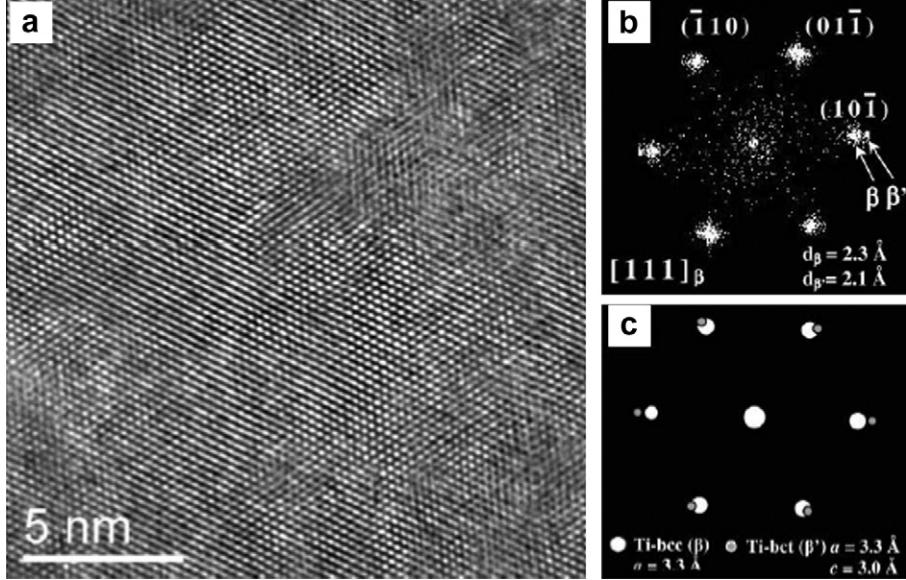


Fig. 11. Phase separation in the beta phase [28] shown by high resolution transmission electron microscopy and related satellite reflections in the Fourier transform of the image (that is, in reciprocal space).

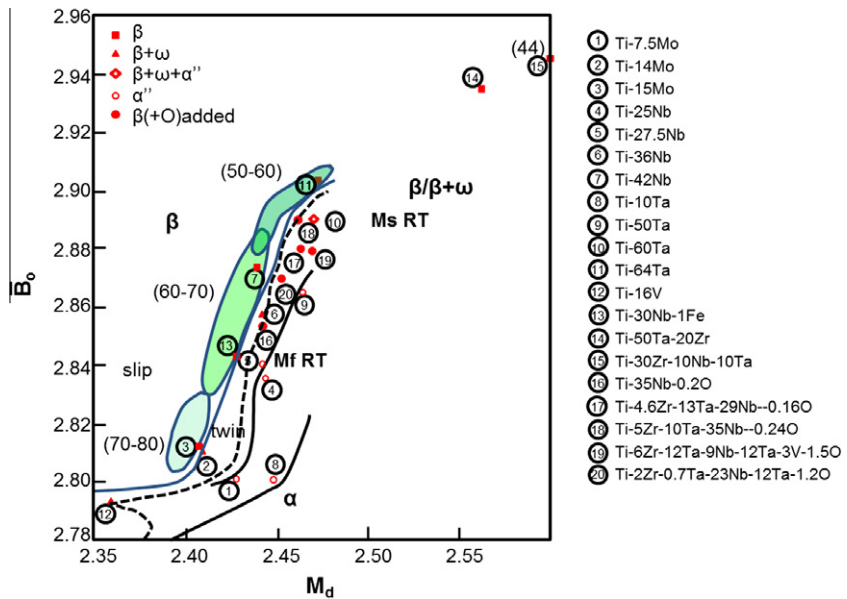


Fig. 12. The Bo–Md diagram [30].

alloys is the barrier to dislocation motion represented by alpha–beta interfaces as we shall describe in greater detail later. Consequently, prediction and control of alpha phase size, morphology and distribution including that of its orientation variants are of fundamental importance in determining the properties of titanium alloys [1].

2.2.2. Martensite

The martensite formed on quenching from the beta phase has the hcp structure (alpha') in beta stabilizer lean alloys but transitions to an orthorhombic structure (alpha'') in beta-rich alloys, as indicated schematically in

Fig. 5. Most features of the crystallography, morphology and composition dependence of these martensite phases are well understood [3] and will not be repeated here. We only emphasize that the transformation involves three distinct processes. The first is the Bain distortion that transforms the cubic lattice to either the orthorhombic or hexagonal lattice. The second is the lattice invariant shear by either twinning or slip to realize the invariant plane. The third is a shuffle that takes place on every alternate (110) plane in a [110] direction, as shown in Fig. 9a, to bring the atoms to their proper positions in the orthorhombic or hexagonal martensite structure. The extent of the shuffle

in the orthorhombic martensite depends sensitively on composition [18]. Since the shuffle can take place in alternate directions for a given martensite plate, a domain structure is realized [19] within the plates (Fig. 9b) with a given direction of shuffle within each domain. If, on the other hand, the shuffle occurs in the absence of the Bain distortion then 12 variants of nanodomains can be formed from opposite shuffle directions for each of the six $\{110\}$ planes, as has been suggested recently [20,21] and as shown in Fig. 9c. These transverse $\{110\}\langle110\rangle$ displacements are associated with $\langle110\rangle$ reirods in reciprocal space, which give rise to diffuse streaking and intensity maxima distinct from reflections associated with the omega phase. This phenomenon is not restricted to titanium alloys and has been observed in other systems in which a parent beta

(ordered or disordered) transforms to martensite at lower temperatures [22].

2.2.3. The omega transformation and phase separation in the beta phase

The transformation of the beta phase to form the omega phase is known to occur by a displacive mechanism involving various degrees of collapse of alternate pairs of (111) beta planes to an intermediate position, which culminates in a region of hexagonal symmetry [1,3]. When the collapse is complete as shown in Fig. 10, the omega phase has a hexagonal structure while a partial collapse results in a trigonal symmetry. The collapse can be described by a displacive wave corresponding to a wavelength equal to $3d_{222}$, and an amplitude of $0.5d_{222}$ for the hexagonal structure (that is, a wave vector of $2/3d_{111}^*$ in reciprocal space). The omega phase is believed to form athermally through a diffusionless transformation on quenching from the beta phase field, and precedes the transformation to orthorhombic martensite at some critical beta-stabilizer content. At higher beta-stabilizer levels the athermal collapse becomes increasingly incomplete. The ratio of d_{0002}^*/d_{222}^* in reciprocal space has been used as a measure of the degree of collapse and varies with composition, as shown in Fig. 10b [23]. When samples containing athermal omega are aged isothermally, the athermal omega can grow rapidly, followed by diffusional rejection of beta stabilizers. Alternatively, isothermal ageing results in the partial (111) collapse proceeding to completion through a coupled diffusional-displacive transformation, as shown by very recent studies using composition-sensitive, high resolution, high angle annular dark field (HAADF) electron microscopy accompanied by atom probe [24].

Fig. 3 also shows equilibrium immiscibility in the beta phase. The chemical spinodal and the associated coherent spinodal can also be present as a non-equilibrium phase separation reaction within the alpha + beta phase field

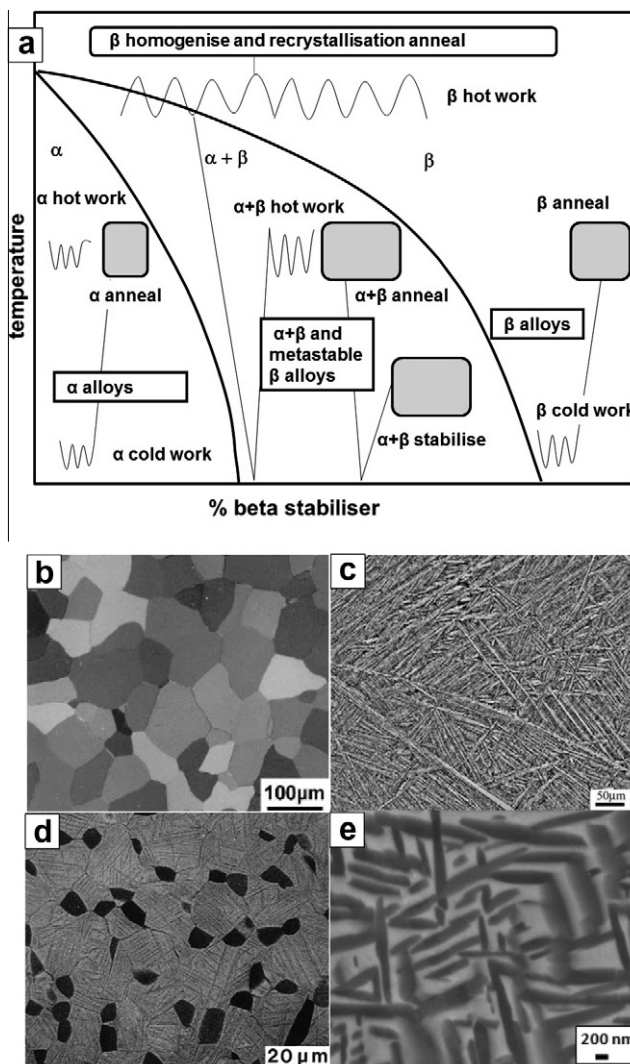


Fig. 13. (a) A schematic diagram showing typical thermomechanical processing sequences. (b) The resulting recrystallized, equiaxed alpha grains in a single-phase alpha alloy [1]. (c) Beta recrystallization followed by cooling into alpha + beta phase field in a near alpha alloy, IMI 834. (d) Equiaxed, primary alpha morphology obtained by alpha + beta processing in a near alpha alloy IMI834 and grains of transformed beta phase ((c,d) courtesy TK Nandy). (e) Fine alpha phase distribution in a metastable beta Ti alloy, Ti-5553 (courtesy Sujoy Kar).

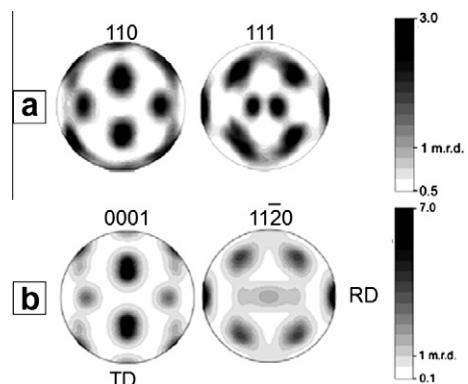


Fig. 14. (a) The texture associated with parent beta before cooling down into the alpha + beta phase field. Two components are seen, a cube component and a gamma component. (b) The consequent texture arising in the alpha phase formed through the Burgers relationship with the intensities weighted for the relative fractions of parent components (adapted from Ref. [37]).

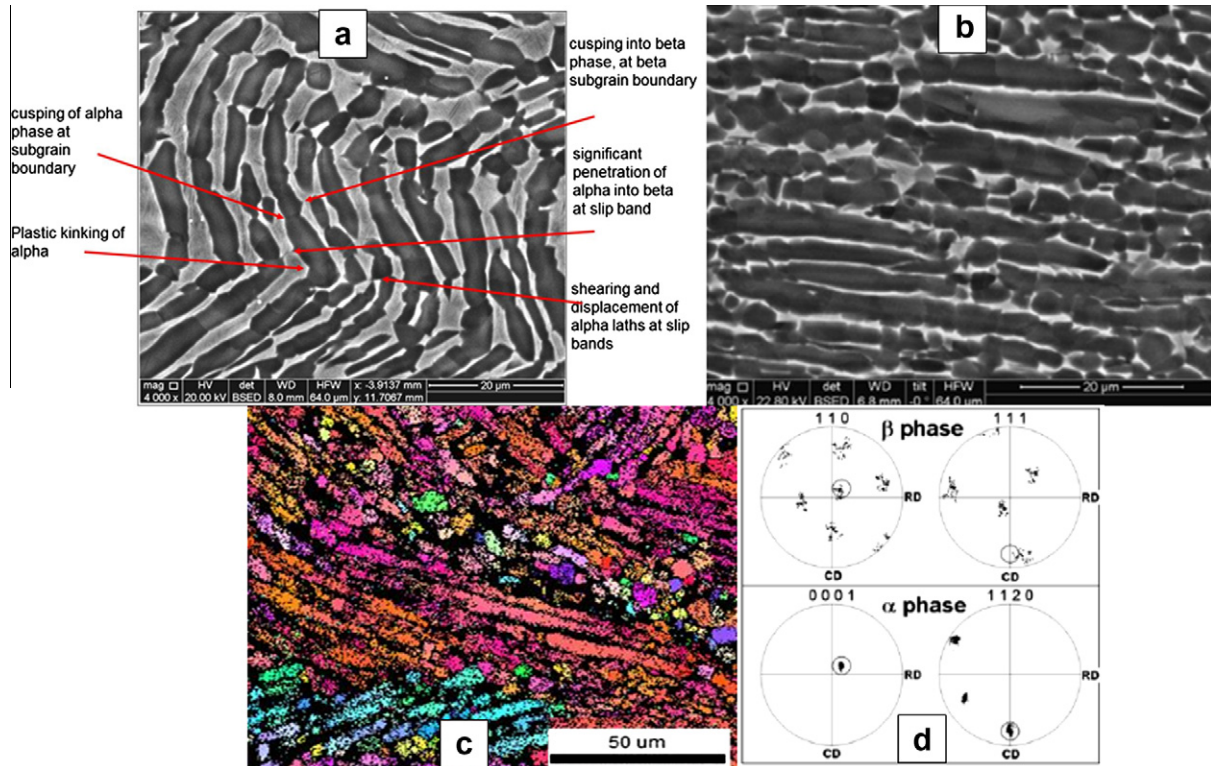


Fig. 15. (a) Alpha lath roughening processes in a near alpha alloy, IMI834, as a result of hot compression in the alpha + beta phase field [126]. (b) Breakdown of laths into globular shapes in the same alloy [126]. (c) OIM of the laths after 0.5% true strain (courtesy B Shanoob). (d) Scatter in alpha orientations after 0.5% true strain in Ti-6Al-4 V (from Ref. [38]).

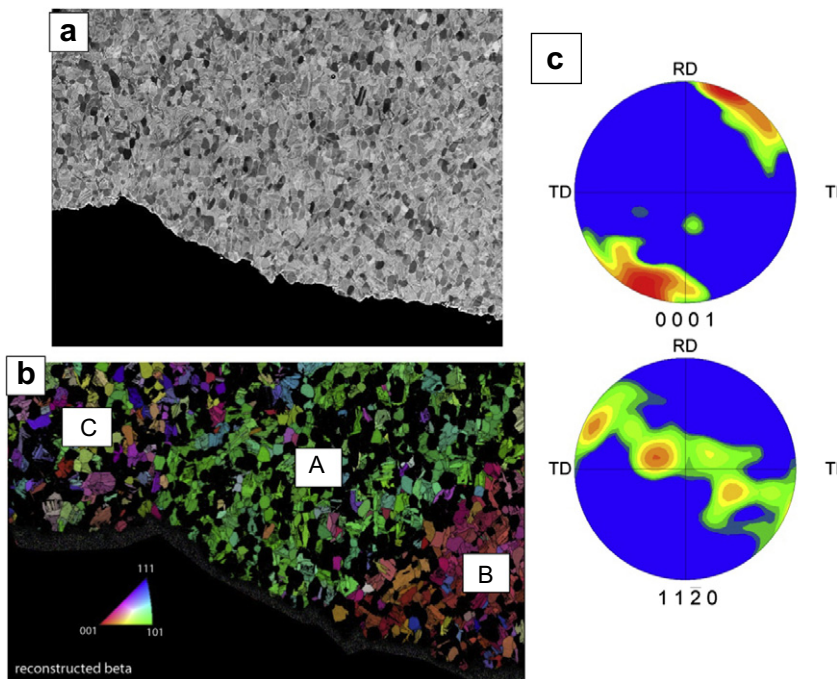


Fig. 16. Microtexture or macrozones in a bimodal structure in a Ti-6Al-4 V alloy: (a) a typical bimodal structure with primary and secondary α in Ti-6 Al-4 V, (b) an orientation image map of reconstructed β orientations (from secondary α and excluding the primary α phase) shows three macro zones, A, B and C. A derived texture map of the primary α phase in zone A shows that all equiaxed alpha particles are similarly oriented [35].

(Fig. 5). The first report of such a phase separation reaction appears to have been that of Harmon and Troiano [25] in

the 1960s. It had been suggested [26,27] a long time ago that the phase-separated regions could serve as nucleation

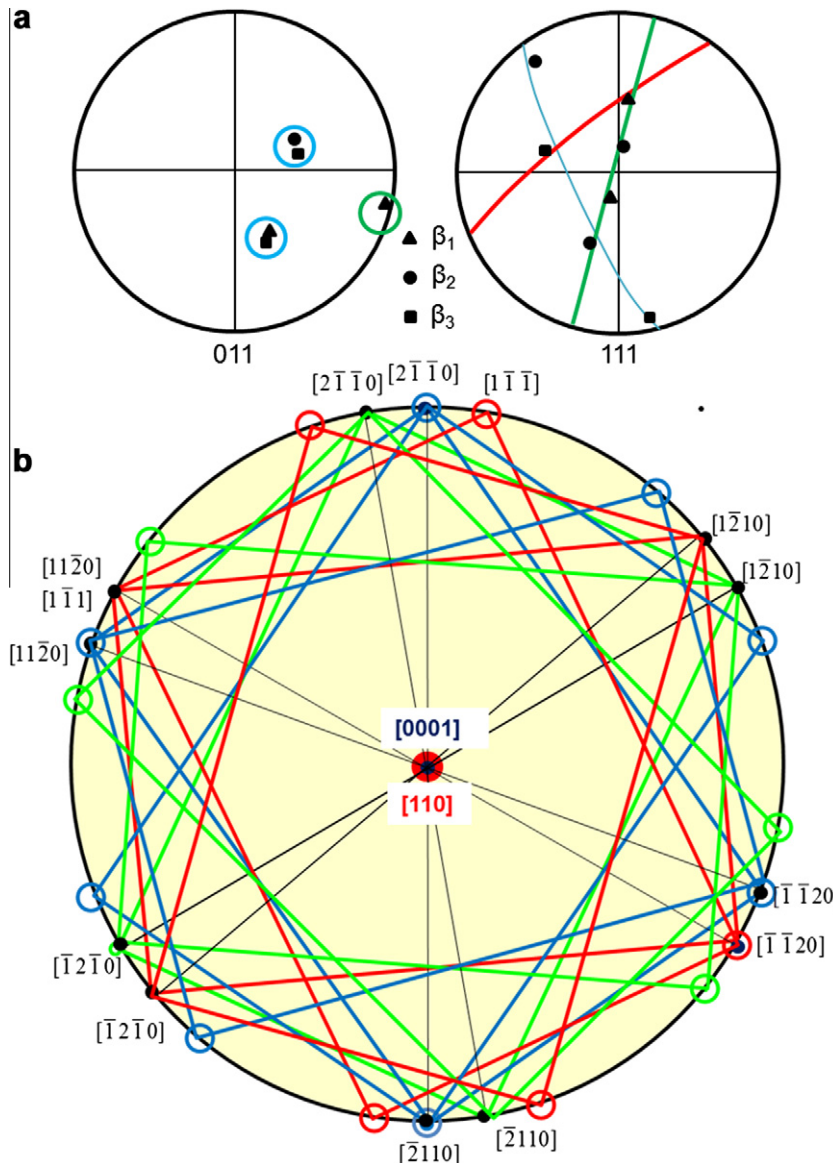


Fig. 17. Special relationships between beta grains in a subtransus processed alloy. (a) This analysis of three beta grains at a triple point by EBSD [35] shows that each pair of grains share very similarly oriented $\langle 110 \rangle$ poles. The $\langle 111 \rangle$ poles normal to these are rotated with respect to each other by 60° or 21° in each case. (b) Two alpha variants (from a beta-to-alpha transformation) can share a common basal plane but are rotated by 10.5° with respect to each other. Six beta variants can arise from each of these alpha variants with a common $\langle 110 \rangle$ plane from the reverse alpha-to-beta transformation leading to 12 beta orientations rotated about a common $\langle 110 \rangle$ direction. These are twin related to each other and rotated to each other by 60° , or multiples of 10.5° .

sites for either the alpha or omega phases depending on the thermal path. More recent studies using high resolution electron microscopy and atom probe microanalysis [28,29] suggest that the phase separation reaction (Fig. 11) may be ubiquitous and can indeed sensitively influence the formation of the omega or alpha phase depending on the cooling rate from the beta phase field or the thermal path on heating to various ageing temperatures within the alpha + beta phase field.

2.2.4. The stability of the beta phase

The Bo-Md diagram [30] (where Bo is the bond order that measures the covalent bond strength between Ti and

any other metal, and Md is the d orbital energy level of the alloying metal) attempts to define the boundaries of the martensite and omega transformations in relation to the modulus of the beta phase using experimental data from a wide variety of alloying systems (Fig. 12).

The preceding discussion has indicated that the beta phase in titanium alloys is unstable relative to a variety of metastable decomposition phenomena at the atomic level. To summarize, these include the Bain distortion for the martensitic transformation that is related to the softening of shear modulus c' and a $\{110\}\langle 110 \rangle$ transverse phonon wave that leads to the shuffle. The latter is a part of the martensitic transformation but can also apparently

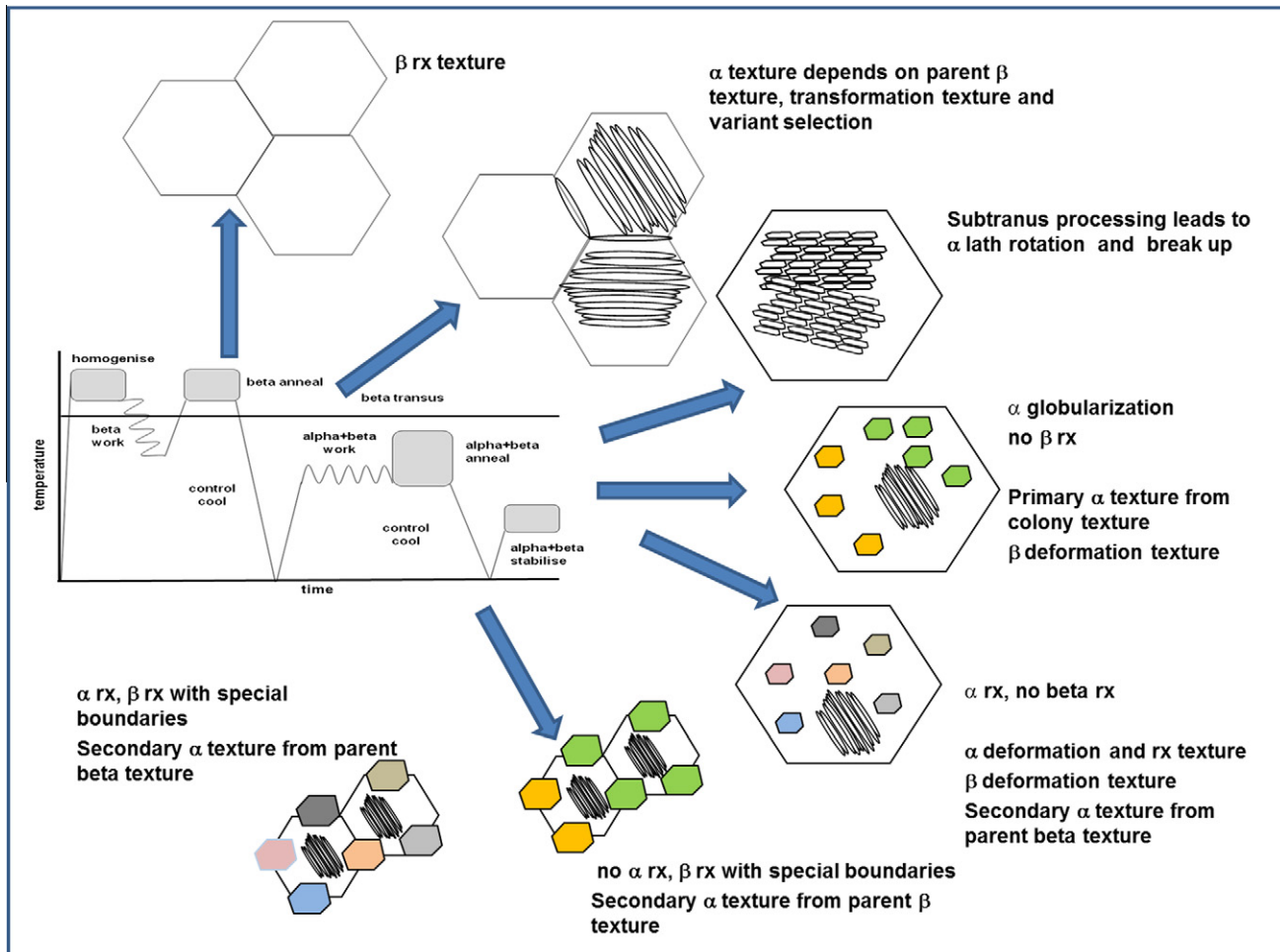


Fig. 18. A schematic indicating processing path and texture development in titanium alloys [35].

occur independently preceding the transformation. In addition, $2/3d_{111}^*$ displacive waves in reciprocal space accomplish the omega transformation while a stress-induced $\{112\}\langle110\rangle$ shear (with an accompanying shuffle) leads to a stress-induced omega phase [3]. Finally, a diffusional (short range) phase separation reaction occurs. The effect of alloying on each of these separate instabilities is incompletely understood at this time. Quite counterintuitively (since they are not beta stabilizers), the elements Al, Zr, Sn, and O in beta solid solution have been shown to retard omega phase formation and decrease the martensitic start temperature, M_s . It has very recently been suggested that O enhances the shuffle associated with the martensite transformation (see Section 2.2.4), while suppressing the Bain distortion [20]. In this context we also note that the mobility of martensite interfaces through beta-phase-containing omega particles and has received very little attention thus far [31].

The emergent area of biomedical applications of titanium exploits the low modulus of beta titanium and shape memory effects related to the martensitic transformation. The physical and mechanical behaviour of beta titanium as related to these instabilities is currently the

subject of significant research effort and will be described in later sections.

3. Processing, structure, texture and microtexture

Thermomechanical processing of titanium alloys involves deformation in the alpha, alpha + beta or beta phase fields depending on the alloying content (Fig. 13). The interaction between the flow process and microstructure evolution has been studied extensively [32–34]. A complex interplay exists between deformation and recrystallization textures of the individual phases, transformation textures arising out of the beta-to-alpha and the reverse alpha-to-beta transformation, and the scale of microstructural evolution [35].

After melting, the as-cast ingot is homogenized in the beta phase field and mechanically worked in the beta phase field to break up the cast beta grain structure, further homogenize the structure and refine the beta grain size. After the initial recrystallization of the beta phase, the material is worked through the transus to retain the refined grain structure. Subsequently, alpha alloys are processed within the alpha phase field by hot or cold deformation,

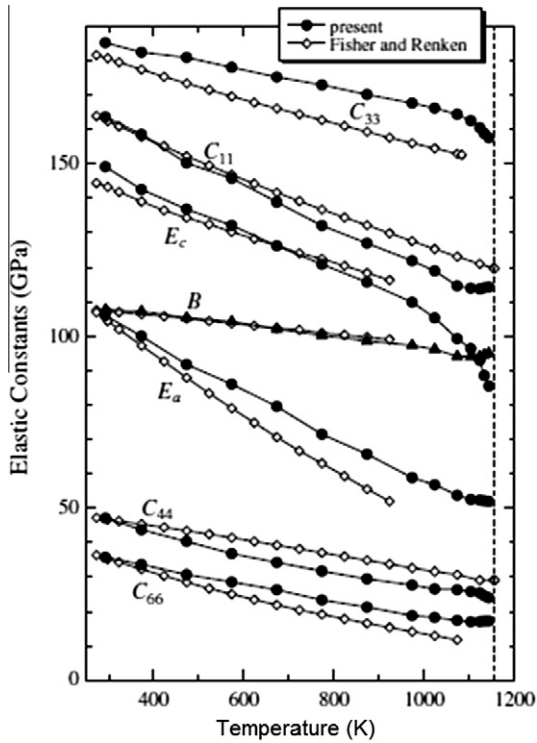


Fig. 19. Elastic constants of the alpha phase as a function of temperature [46].

combined with annealing treatments, to control the alpha grain size and texture. On the other hand, alpha + beta or metastable beta alloys can be processed in the two-phase alpha + beta phase field to transform the lamellar alpha phase into equiaxed forms, thus deriving additional microstructural variability in controlling properties. Beta alloys are processed in the single-phase beta region primarily to enable grain size control. Typical microstructures from different processing sequences are also shown in Fig. 13. A detailed description of resulting deformation and recrystallization textures is available in Singh and Schwarzer [36]. We focus in this section primarily on the relationship

between microstructure evolution and microtexture in alpha + beta alloys that has emerged in recent years. Awareness of the presence and nature of microtexture (or macrozones) is relatively recent, enabled by the evolution of electron backscatter diffraction (EBSD) techniques in the scanning electron microscope (SEM).

When the parent beta grains are textured by the beta deformation process, the alpha plates that form on cooling into the alpha + beta phase field (Fig. 13c) inherit some aspects of this texture due to the BOR. Fig. 14 is an example from the work of Lonardelli et al. [37]. The product phase texture can arise from an equivolume distribution of the 12 variants, or can be influenced by a variant selection process such as that arising from side plates emerging from grain boundary alpha, as described earlier.

Most alpha + beta alloys are subsequently processed below the transus to break down the lamellar alpha structure to a globular or equiaxed form after recrystallization, and in their fully heat-treated condition will consist of controlled volume fractions of the globular and lamellar components of alpha structure (bimodal structures) or globular alpha and retained beta phase, depending upon alloy composition and heat treatment (Fig. 13d and Fig. 31). Both alpha lath breakdown and recrystallization and recovery and recrystallization of the beta phase, can occur during sub-transus processing. Fig. 15 illustrates various processes: alpha laths can plastically kink and bend, a process favoured at relatively low temperatures and when the long dimension of the laths is oriented parallel to the compression axis. They tend to rotate to lie normal to the compression axis [38]. In addition, the alpha/beta interfaces roughen due to a grooving process described by Margolin and Cohen [39] and Weiss et al. [40]. The lath roughening and breakdown process to a globularized form is dependent on the amount of strain, the initial alpha lath size and orientation, and initiates at strains of ~ 0.5 and is completed at strains of ~ 2.5 [41–43]. Experimental observations show a correlation between the initial lath width and resulting equiaxed grain

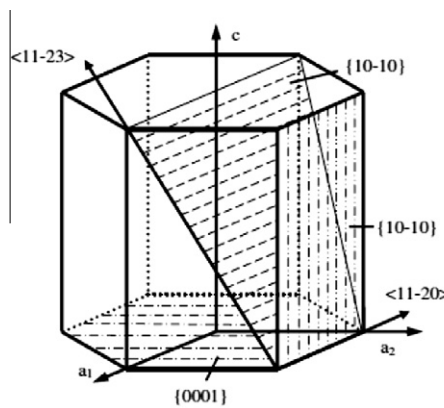


Fig. 20. Slip systems in the alpha phase and the variation of CRSS with temperature [1] with recent data from high purity Ti [53] superimposed as data points in red. (For interpretation of the references to colour in this figure legend, the reader is referred to the web version of this article.)

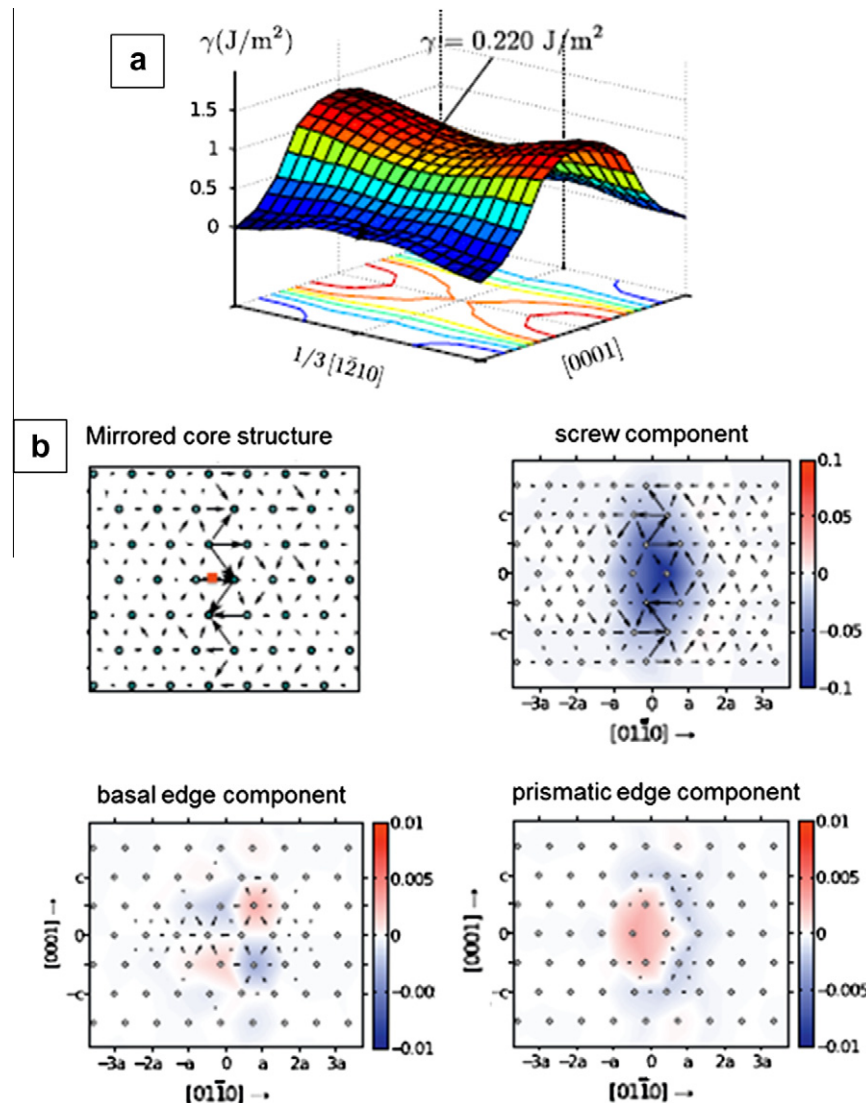


Fig. 21. The core structure of screw “a” dislocations in the alpha phase [52]: (a) the generalized stacking fault energy surface from DFT, (b) the low energy core structure showing partial differential displacements (arrows) and contour plots of the Nye tensor.

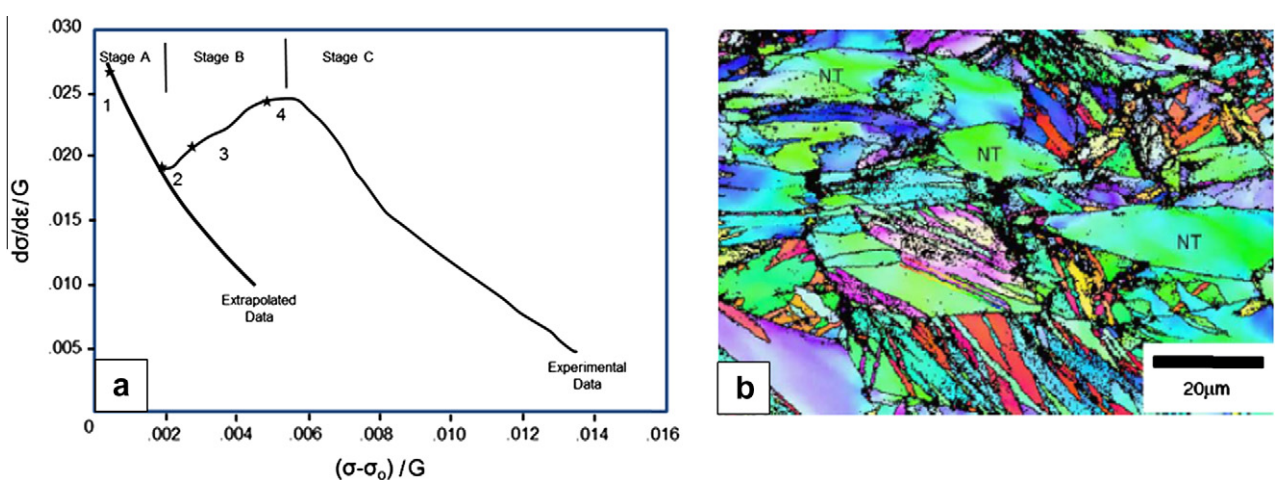


Fig. 22. (a) The three stage stress–strain curve associated with twinning in alpha titanium [54]. (b) Twinning in alpha phase after cold rolling [57].

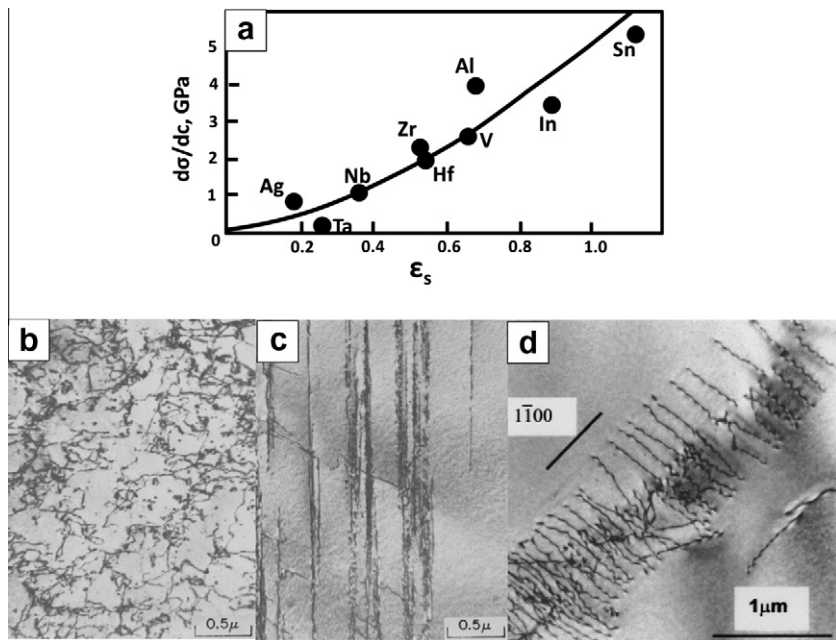


Fig. 23. (a) Solid solution strengthening of the alpha phase by substitutional solutes [59] as a function of strengthening parameter related to interaction with screw dislocations. (b–d) The effect of O and Al on slip character in titanium: (b) pure Ti with 475 wppm O [63], (c) Ti with 5200 wppm O [63], (d) Ti–5 wt.% Al [49].



Fig. 24. Aircraft hydraulic tubing (Ti–3Al–2 V) cracked in bend tests (courtesy Defence Metallurgical Research Laboratory, India).

size [1]. No quantitative, physics-based models for the alpha globularization process exist at this time.

The equiaxed grains that form as a result of globularization of a parent alpha colony can be similarly oriented to these laths after a range of processing conditions (see Ref. [44] for an example in aeroengine disc profiles). This leads to “macrozones” or microtextured areas of similarly oriented equiaxed alpha phase associated with the original colony size. An example of similarly oriented alpha phase particles within a prior beta grain of beta is shown in Fig. 16. The beta grains associated with these macrozones are significantly smaller than the starting beta grain size, but are nevertheless very often related to each other by specific orientations [13] involving rotations about a common $\langle 110 \rangle$ axis, as shown in Fig. 17. The origin of these special

orientations is not completely clear. It is, however, most likely that these special textures arise from recrystallization of the beta phase within the two-phase region with an epitaxial relationship (in the Burgers orientation) with the alpha grains [45]. Six beta variants can form with a common $\{110\}$ plane from a single parent alpha grain. Since two alpha laths formed from parent beta can themselves share a common $\{0001\}$ plane, it is possible to realize 12 beta variants with a common $\{110\}$ plane as shown in Fig. 17.

Fig. 18 describes schematically the sequence of microstructure development with processing along with a description of accompanying texture. A complete understanding of the plasticity of these materials and their fracture will depend on the ability to model these microstructural variants and their underlying texture.

4. Mechanical behaviour

4.1. Alpha titanium

The most recent determination of elastic moduli of alpha titanium appears to be that of Ogi et al. [46] and these are shown in Fig. 19. The Young’s modulus in the “c” direction is higher than that in the “a” direction. The anomalous behaviour just below the transformation temperature to the beta phase is attributed to premonitory effects associated with the softening of elastic constants that enable the transformation to proceed via the Burgers mechanism. Elastic constants obtained from first principles calculations are reported by Hao et al. [47]. The plastic behaviour of alpha titanium is extremely anisotropic as

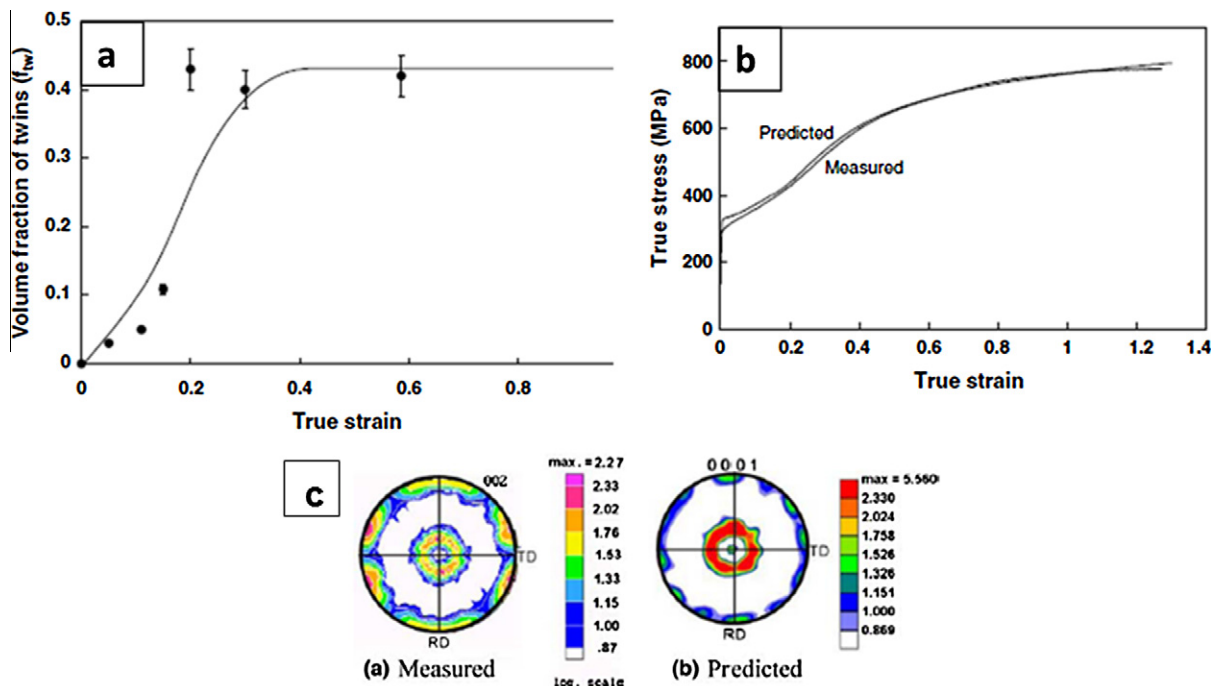


Fig. 25. Crystal plasticity finite element predictions of the deformation behaviour of alpha Ti using a Taylor model [67]: (a) the prediction of twin volume fraction with strain in alpha Ti in uniaxial compression, (b) the prediction of the stress–strain curve, (c) the prediction of texture.

well. Fig. 20 shows possible slip systems in titanium and the variation of critical resolved shear stress for different slip systems with temperature. Tanaka and Conrad [48] summarize early data on single crystal alpha titanium at low temperatures. Their work shows that “a” slip is easiest on prismatic planes but the ratio of critical resolved shear stress (CRSS) on the basal and pyramidal planes to the prismatic plane decreases with increasing interstitial content and Al content [49]. Prismatic “a” slip has therefore been extensively studied. The prismatic stacking fault associated with the dislocation core has the lowest energy for the “a” dislocation, and it has been found that flow on the prismatic plane is controlled by low mobility of screw dislocations arising from non-planar core structures [50–52], shown from recent computations in Fig. 21. CRSS data generated more recently from microbeam tests in high purity alpha titanium [53] are superimposed on earlier data from Ti-6 wt.% Al in Fig. 20. In orientations that do not allow “a” slip, that is, orientations with the “c” axis along the stress axis, alpha titanium responds by twinning on $\{10\bar{1}1\}$, $\{10\bar{1}2\}$, $\{11\bar{2}1\}$ and $\{11\bar{2}2\}$ planes depending upon whether the loading stresses are tensile or compressive (see Ref. [1] for a more detailed description).

The combination of “a” component slip and twinning in pure titanium leads to polycrystalline behaviour with three stages of strain hardening [54–56] (Fig. 22a). Twinning may affect the flow stress due to a Hall–Petch type mechanism, a “Basinski” mechanism in which glissile dislocations in untwinned areas are converted to sessile dislocations after twinning, and finally geometric softening due to reorientation of twinned areas. The subsequent decline in strain

hardening is due to a saturation of the twin volume fraction. In temperature and compositions regimes where twinning is absent, titanium can be hardened through grain size strengthening with values of k_y , the Hall–Petch coefficient, ranging from ~ 0.5 to $0.7 \text{ MN m}^{-3/2}$. Similarly, cold rolling results in twinning (Fig. 22b) to provide an adequate number of independent shear systems [57], and at very high reductions shear bands are initiated when twinning is saturated. Twinning introduces a basal component of texture normal to the rolling plane.

The alpha phase can be significantly hardened by interstitials such as oxygen [58] and by substitutional solutes, among which the most common are Al, Sn and Zr [59] (Fig. 23a). Alpha titanium also exhibits well characterized dynamic strain ageing effects that may be attributed to interstitials such as oxygen, nitrogen, carbon or Si [60,61]. The addition of Al or O suppresses twinning, and also changes slip character [49,62,63] to planar configurations (Fig. 23b). In the former case, slip planarity is believed to originate from slip plane softening caused by the destruction of short-range order induced by Al. Many years ago Churchman suggested [64] that ordering of oxygen in interstitial sites would result in interference with slip on basal and prismatic planes. When both Al and O are present there is a synergy between them that intensifies planar slip. The way an interstitial solute (O) and a substitutional solute (Al) can interact to affect slip is not understood. We shall see later that planar slip on basal planes is associated with faceted crack initiation on these planes in fatigue.

The effect of alloying additions on core spread of the “a” dislocation does not appear to have been explored at all

Periodic Position	Element	Biocompatibility	Carcinogenic	Genotoxic	Mutagenic	Cytotoxic	Allergenic	Corrosion Prone	Other
3d	Ti	Yes	No	No	No	Med	No	No	No
	V	No	Yes	Yes	Yes	High	Disputed	No	No
	Cr	No	Disputed	Yes	Yes	High	Yes	No	No
	Mn	No	No	Yes	No	High	No	Yes	No
	Fe	No	No	Yes	Disputed	Med	No	Yes	No
	Co	No	Yes	Yes	Yes	High	Yes	Yes	Yes
	Ni	No	Yes	Yes	Yes	High	Yes	Yes	Yes
	Cu	No	No	Yes	Yes	High	Yes	Yes	Yes
4d	Zr	Yes	No	No	No	Low	No	No	No
	Nb	Yes	No	No	No	Low	No	No	No
	Mo	No	Disputed	Yes	Yes	Low	Yes	Yes	Yes
	Tc	No				Radioactive			
	Ru	Yes	No	No	No	Med	No	No	Yes
	Rh	No	Yes	Yes	Yes	High	Unknown	No	No
	Pd	No	Yes	No	Disputed	Med	Yes	No	No
	Ag	No	No	No	No	High	Yes	No	Yes
5d	Hf	Unknown	Unknown	Unknown	Unknown	Med	No	No	Unknown
	Ta	Yes	No	No	No	Low	No	No	No
	W	No	Yes	Yes	No	Med	No	Yes	No
	Re	Unknown	Unknown	Unknown	Unknown	Unknown	No	No	Unknown
	Os	No	Unknown	Yes	Yes	High	No	Yes	No
	Ir	No	No	No	Yes	High	No	No	Yes
	Pt	No	Yes	Yes	Yes	High	Yes	No	No
	Au	Yes	No	No	No	High	No	No	No
Other	Al	No	No	Yes	No	Low	No	No	Yes
	Zn	No	No	No	No	High	No	No	Yes
	Sn	Yes	No	No	No	Low	No	No	Yes

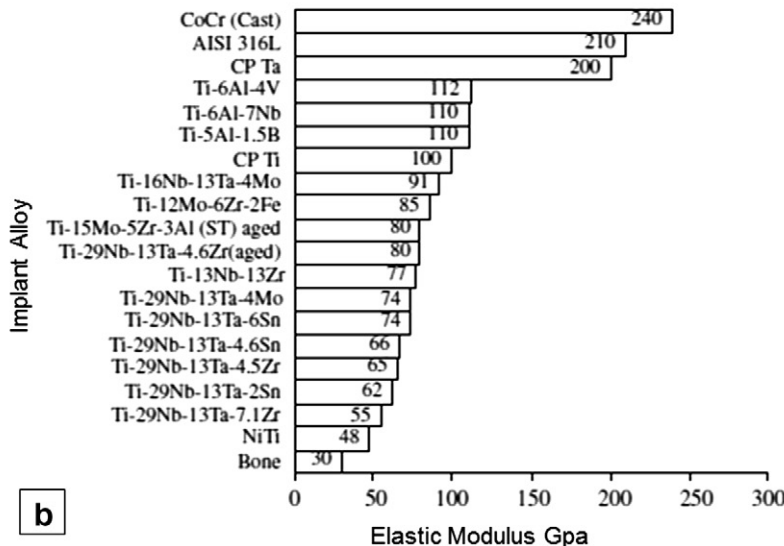
a**b**

Fig. 26. (a) The biological impact of metals [72]. (b) The modulus of various alloys in relation to bone [73].

(see for example Ref. [65] for the most recent discussion), although these effects would appear to be fundamental to alpha phase plasticity. Nor has the combined and interactive effect of grain size, strain rate and alloying on the twinning regime been quantified. In alpha titanium that contains Al and/or oxygen, the decreased frequency of twinning is compensated for by the operation of non-basal “c + a” slip. Since the critical resolved shear stress for “c + a” slip is considerably higher than that for “a” slip (Fig. 20), significant texture strengthening can occur when the loading direction imposes stress parallel to the c-axis. If for example texture is such that the c-axis of the grains is

largely oriented perpendicular to the plane of the sheet in sheet forming operations, the material is then stronger in the through-thickness direction, which in turn improves formability by minimizing through-thickness thinning. This is important in welded tubing made from strip, an example of which is shown in Fig. 1a. Seamless tubing is made by extrusion and pilgering for use as hydraulic tubing in aircraft. Deformation texture also affects the properties of such tubes (Fig. 24) through preferred orientation induced by the forming operations.

In view of the importance of alpha phase deformation on mechanical behaviour, various attempts have been recently

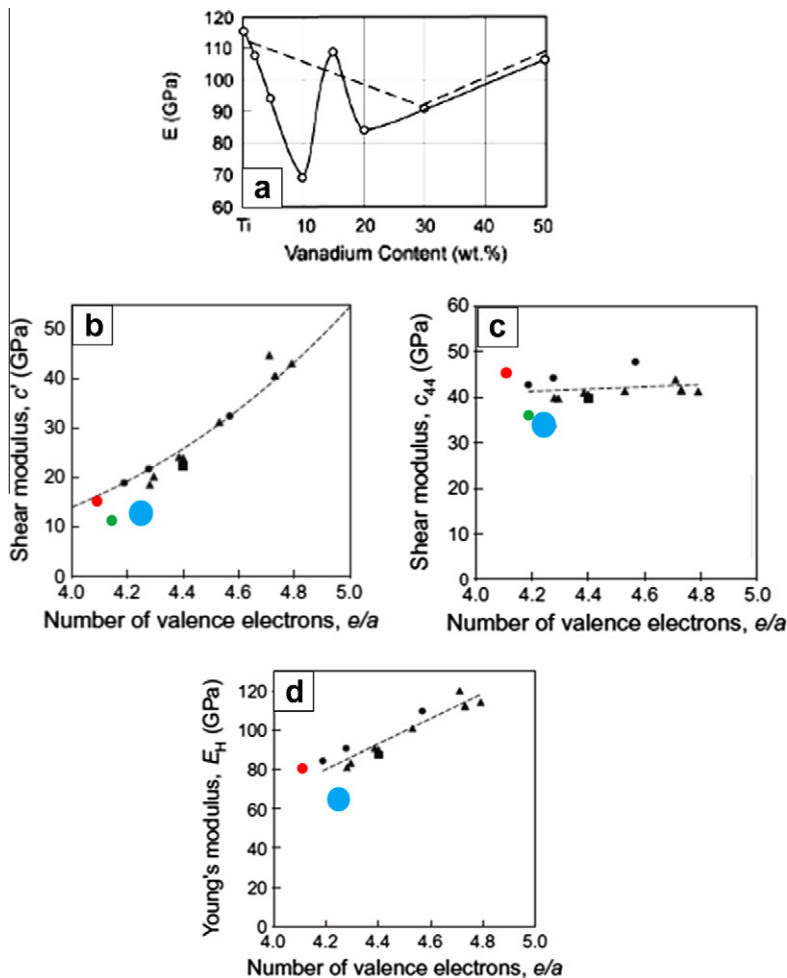


Fig. 27. (a) The variation of Young's modulus with beta alloying addition (from Ref. [1]). (b) The variation of c' with e/a ratio. (c) The variation of c_{44} with e/a ratio. (d) The variation of Young's modulus (deduced from single crystal constants) with e/a ratio. (b–d) are adapted from Ref. [74] with data included from Ti-15Mo-5Zr-3Al (red) [77], Ti-24Nb-4Zr-8Sn (green) [76] and gum metal (blue) [75]. (For interpretation of the references to colour in this figure legend, the reader is referred to the web version of this article.)

made using a variety of modelling approaches to capture the different aspects of alpha titanium plasticity described above. Nixon et al. [66] used a computationally less demanding, continuum mechanics model that captures the tension-compression asymmetry of twinning by a function that defines a fully 3-D orthotropic yield criterion, and hardening which describes the evolution of this orthotropic yield surface with equivalent strain. Taylor type crystal plasticity models that capture the phenomenology of twinning described earlier are used to model the strain hardening of polycrystals by Salem et al. [67] while grain size and orientation distribution models have been explored by Bradley et al. in the slip regime [68]. Heterogeneity in strain at the grain level has been captured through a crystal plasticity finite element model [69,70] incorporating anisotropy in slip and twinning as a unidirectional slip system. Hardening in single crystals oriented for prismatic slip and the transition from Stage I to Stage II has been modelled [71] by expressions for deformation kinetics that allow for differential velocities of edge and screw components of prismatic

“a” dislocations. Fig. 25 shows an example of modelling prediction in comparison with experimental results.

4.2. Beta titanium

A widening area of application of titanium alloys is in biomedicine [72,73], covering dental implants, parts for orthodontic surgery, joint replacement parts (of which Fig. 1d is an example) and bone fixation devices, housing for pacemakers and artificial heart valves, surgical instruments, components in high-speed blood centrifuges, and shape memory related applications as stents, orthopedic staples and even occluding structures to heal congenital heart defects. Biomedical implants can fail in service in a variety of ways including wear and corrosion, fibrous encapsulation, inflammation and mechanical failure, and importantly a modulus mismatch between bone and implant [73]. The biocompatibility of various metals and a comparison of various alloys to the modulus of bone are shown in Fig. 26. Ti is attractive in both these aspects and

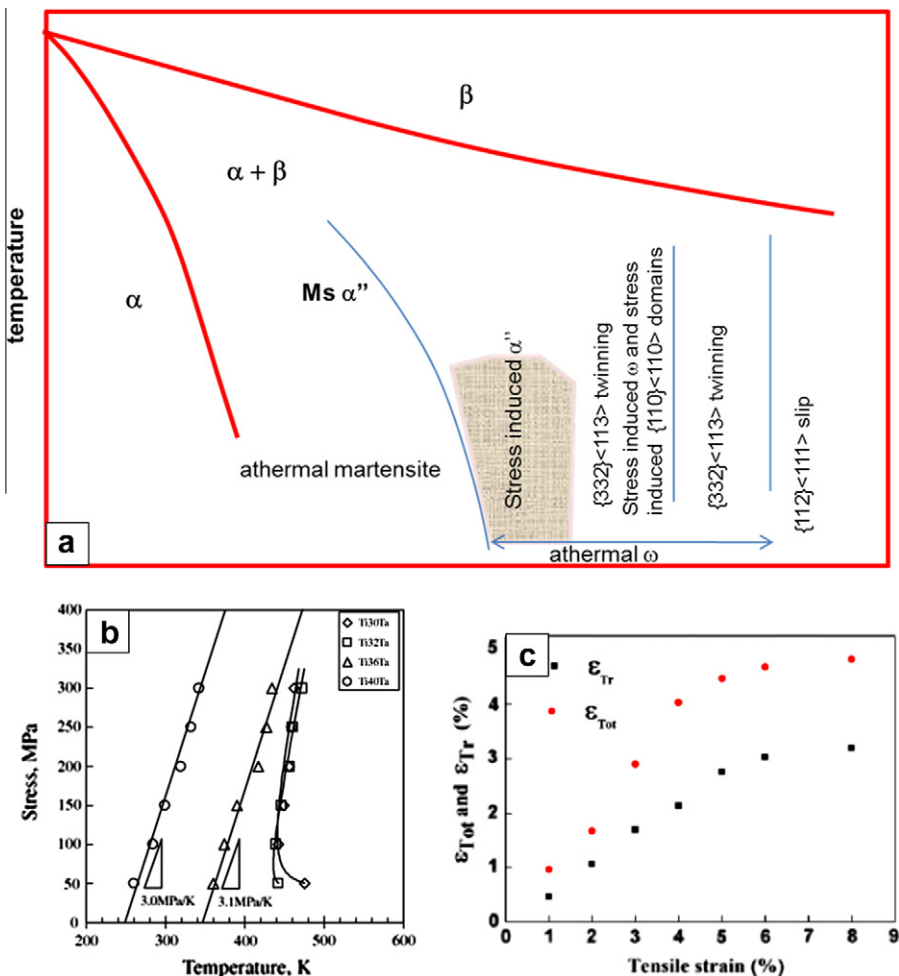


Fig. 28. (a) A schematic description of the effect of beta alloying content on beta phase deformation response. (b) The effect of stress on the M_s of Ti-Ta alloys [81]. (c) The total recovered strain and the recovered anelastic strain in a Ti-7.5Nb-4Mo-1Sn alloy [79].

the modulus of the beta alloys approaches that of bone. It is this latter requirement that has driven a greater understanding of understanding of the stiffness of the (relatively low modulus) beta phase as a function of type and concentration of alloying additions.

The beta phase is unusual in that its modulus depends significantly on alloy composition. The typical dependence of Young's modulus with beta-stabilizing addition is shown in Fig. 27a. At low beta-stabilizing contents, M_s lies above room temperature and the decrease in modulus with alloying reflects the modulus of martensite and any untransformed low modulus beta phase (which increases with alloying addition). With further alloying the beta phase becomes unstable with respect to the formation of nano-scale athermal omega, resulting in the subsequent peak in modulus. At still higher alloying content the values reflect that of the retained metastable or stable beta phase and are significantly lower than that of the alpha phase. The dashed line indicates the modulus values of the annealed structure and therefore that of a two-phase alpha + beta phase structure with alloy compositions corresponding to the alpha/alpha + beta/beta phase boundaries, and is consistent with the rule of mixtures.

Fig. 27b-d shows the various moduli derived from single crystal data [74–78] as a function of electron/atom ratio. The shear modulus, c' , decreases as a function of e/a ratio while c_{44} remains a constant. Both c' and c_{44} fall with decreasing temperature until the athermal omega start temperature or the M_s is reached. Indeed c' is an indicator of the stability of the beta phase since the softening of c' provides the basis for the martensitic transformation. The bulk modulus does not vary with e/a ratio. We note that decreasing the e/a ratio also raises the M_s and athermal ω_s temperature, and therefore alloy design towards low modulus alloys attempts suppress these transformations below room temperature at the lowest possible e/a ratio. However, it is appropriate to caution the reader that assignment of valence to transition metals with unfilled d shells in the electronic structure can be problematic. This is particularly true when one of the alloying additions is present an interstitial, such as O or N. Fig. 27 indicates that compositions based on the Ti-Nb-Ta-Zr and Ti-Nb-Ta-Zr-Sn have c' and c_{44} values that are lower than the trend would suggest in terms of the e/a ratio and the composition of "gum" metal (which additionally contains deliberate additions of O) falls into this class [75],

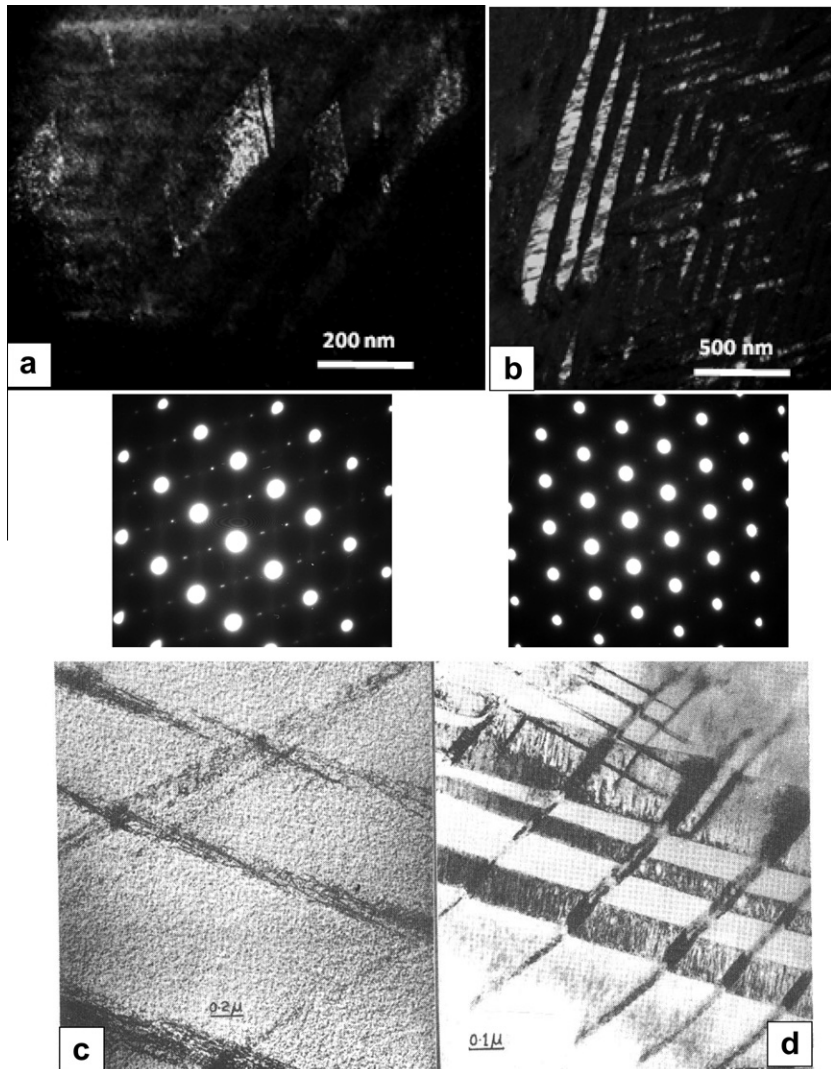


Fig. 29. The formation of stress-induced omega (a) and martensite (b) in a gum metal alloy composition [127], (c) $\{110\}\langle 111 \rangle$ slip and (d) $\{332\}\langle 113 \rangle$ twinning in a Ti–15V–3Al–3 Cr–3Sn alloy deformed at room temperature and 83 K respectively [128].

apparently because Zr, Sn and O all suppress the omega and martensitic transformation. Clearly, elastic constants will depend in a complex manner on the variety of instabilities that the beta phase is subject to over these ranges of e/a ratio, as described in Section 2.2.4, and we suggest that a truly fundamental understanding of these effects in relation to alloying is still lacking at present.

Fig. 28a schematically summarizes the variety of inelastic responses of the beta phase to stress. Concerns of biocompatibility related to the Ni present in the common Nitinol shape memory alloys (Fig. 26) has led to a greater exploration of shape memory behaviour in Ti alloyed with other more compatible elements [73]. A shape memory effect (as well as superelastic behaviour, of which Refs. [79–81] are just examples) can be realized in the regime where M_s of the beta phase lies near room temperature as demonstrated now in a wide variety of alloys (Fig. 28b and c). These include relatively high temperature shape memory effects as in Ti-Ta alloys [81]. As with all shape

memory transformations factors related to phase stability and the yield stress of the parent beta phase play a critical role in determining the recoverable strain, the work output and the domain for stress-induced transformations. In particular for titanium alloys, the formation of thermally induced omega during temperature cycling or the presence of athermal omega will affect both the shape memory effect and superelasticity.

The emergence of gum metal [82] as a subset of alloys that display superelastic behaviour has spurred considerable work in understanding inelastic behaviour in this class of alloys. In addition to superelastic properties, gum metal (especially when cold-worked) combines very low modulus with ultrahigh strength, and displays an invar-like effect at around room temperature. When originally announced, it was proposed that the strength of cold-worked gum metal approaches the ideal shear strength of the alloy determined by the shear modulus along the $\langle 111 \rangle$ direction. As a consequence, it was suggested that gum metal does not

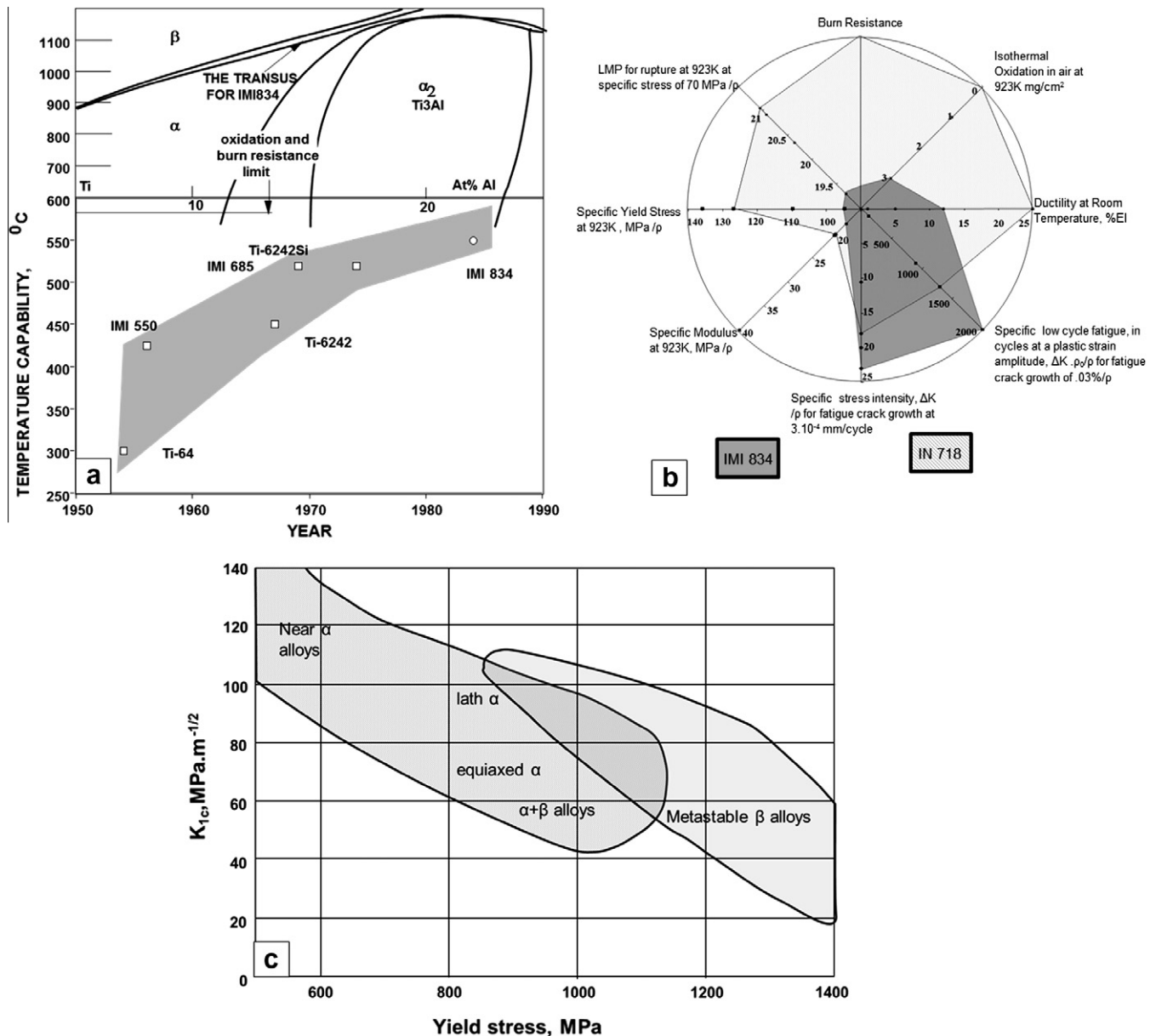


Fig. 30. (a) The temperature capability of titanium alloys. (b) The specific properties of the IMI 834 alloy in relation to the nickel base alloy IN718 at 923 K. (c) The fracture toughness of titanium alloys in relation to their yield strength [129].

deform by conventional dislocation mechanisms or the formation of stress-induced products but by an elastic instability leading to the occurrence of localized shear or “giant faults” [82,83]. The key ingredients in this process were visualized to be (a) the adjustment of the e/a ratio of the composition to a value of 4.24 at which c' theoretically approaches zero, leading to a low shear modulus (b) the strengthening of the alloy through oxygen additions; (c) the preference of shear over cleavage under conditions approaching the ideal shear strength, and finally (d) the dissipation of localization at grain boundaries, permitting hardening. It was proposed that ideal shear strength could be approached through oxygen additions as a consequence of oxygen clustering and interaction with the stress field of

dislocations, or the presence of omega phase or the formation of nanodomains associated with the $\{110\},\langle 110\rangle$ shuffle (described earlier). It must be noted that the ideal shear strength is relatively low in these alloys in a conventional sense because c' has a low value, but is still high in relation to conventional yield.

However, it has also been suggested in later work (see Ref. [84] for example) that since the experimentally measured c' does not actually approach zero the ideal shear strength is still relatively high compared to the observed strength of gum metal and the superelastic behaviour is better explained by more conventional deformation mechanisms arising from slip, twinning and stress-induced martensite or omega formation (Fig. 29a and b). It is clear that

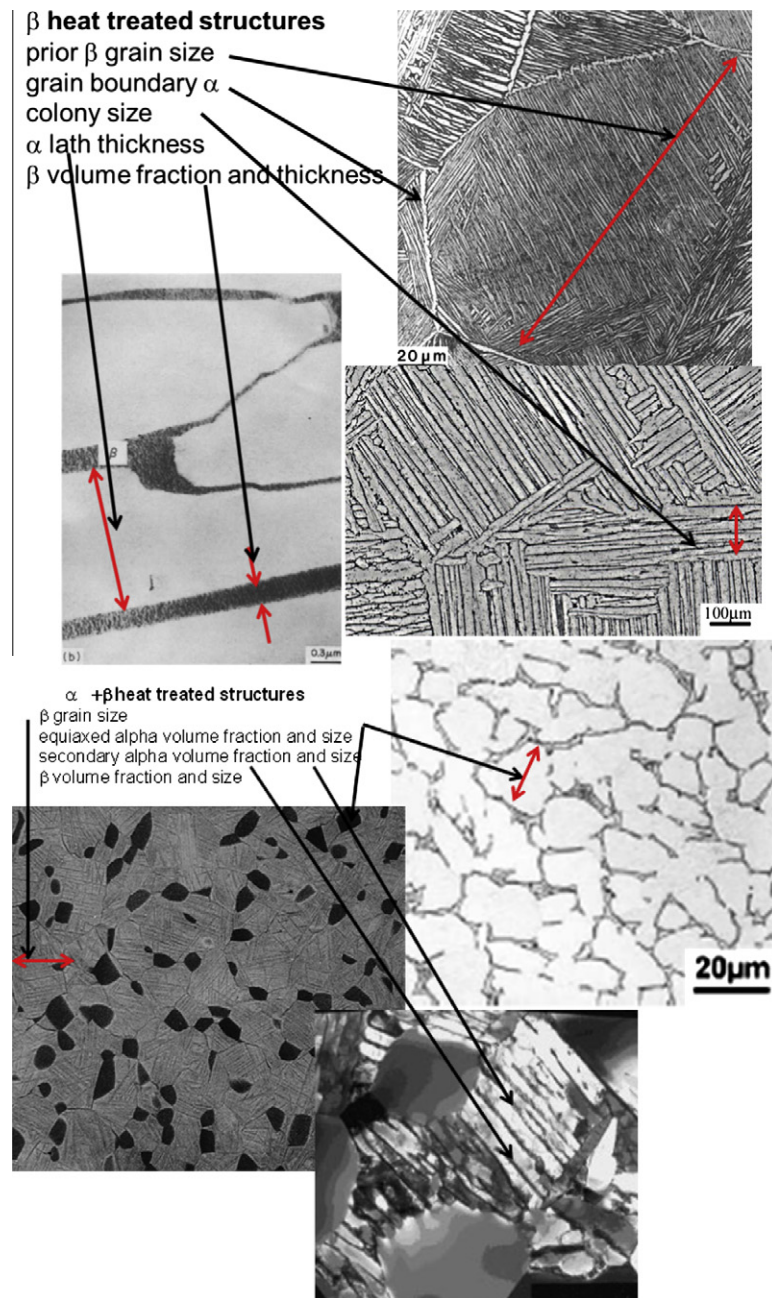


Fig. 31. Example of key microstructural parameters in various classes of microstructures observed in a wide range of titanium alloys.

the issue is still not satisfactorily resolved in spite of significant efforts over the last few years, and we have referred to only a few of the many studies on the subject. We also wish to emphasize the complexity involved in this subject [84]. The composition of gum metal is such that both the lattice distortion and the degree of shuffle associated with the martensite transformation are very low. Consequently, the martensite almost approaches the structure of the parent beta phase, that is, the transformation strain is very nearly a small, pure Bain strain. As a result, the martensite may be untwinned with no requirement of a lattice invariant deformation and there may be high degree of coherence between the parent phase and martensite. This may

obscure the normal signatures of the stress-induced martensitic transformation. The parent phase may itself be heterogeneous at the nanoscale with the presence of omega, oxygen clusters or nanodomains that arise from different variants of the $\{110\}\langle110\rangle$ shuffle. Indeed, it has been recently suggested in one case of a metastable beta alloy containing oxygen that pseudo-elasticity arises from a redistribution of these variants rather than the formation of a stress-induced martensite [20]. A strong effect of beta grain size on the triggering stress for stress-induced martensite has also been documented [85]. Finally, it has been pointed out that observation of structure by transmission electron microscopy can be influenced by the mode of thin

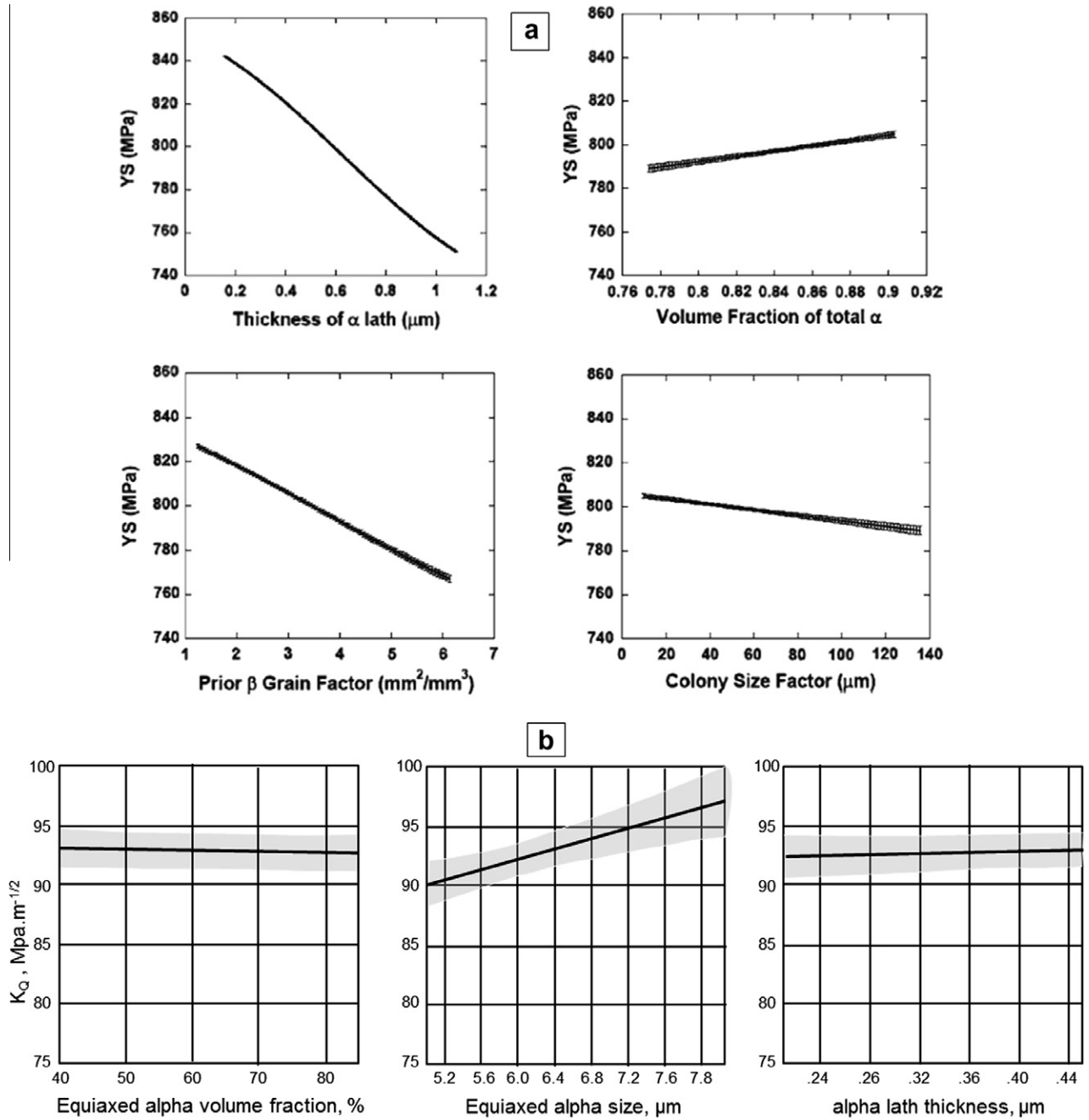


Fig. 32. Neural network analysis shows the trends in the relationship between microstructure and properties in (a) yield strength in a beta heat-treated Ti-64 [89] and (b) fracture toughness in alpha + beta heat-treated Ti-64. This figure shows trends after normalizing for the effect of structure on continuum variables (yield strength) that determine toughness [91].

foil preparation [21], reminiscent of the early days of transmission electron microscopy investigations of metastable beta alloys.

There does, however, appear to be a consensus that oxygen increases the critical stress for martensite formation and will reduce or suppress its formation and that nitrogen behaves in a similar manner [80]. This complex interplay of compositional sensitivity, microstructure and crystallographic effects, and artefacts of characterization, continues to challenge the emergence of clear explanations of the remarkable behaviour of gum metal.

Hanada and Izumi, in a series of early papers [86–88], have clarified deformation mechanisms in compositions that are somewhat richer in beta stabilizing content than have been discussed above (in the sense that stress-induced martensite does not occur). The ratio of the reciprocal distance $d_{0002}^* \omega/d_{222}^* \beta$ measured from electron diffraction patterns in the $<110>$ axis can be used an index of the deviation of the omega phase from the hexagonal structure to trigonal symmetry (and an index of beta phase stability) defined by different extents of collapse of adjacent (111) planes of the beta phase (Fig. 10). The ideal hexagonal

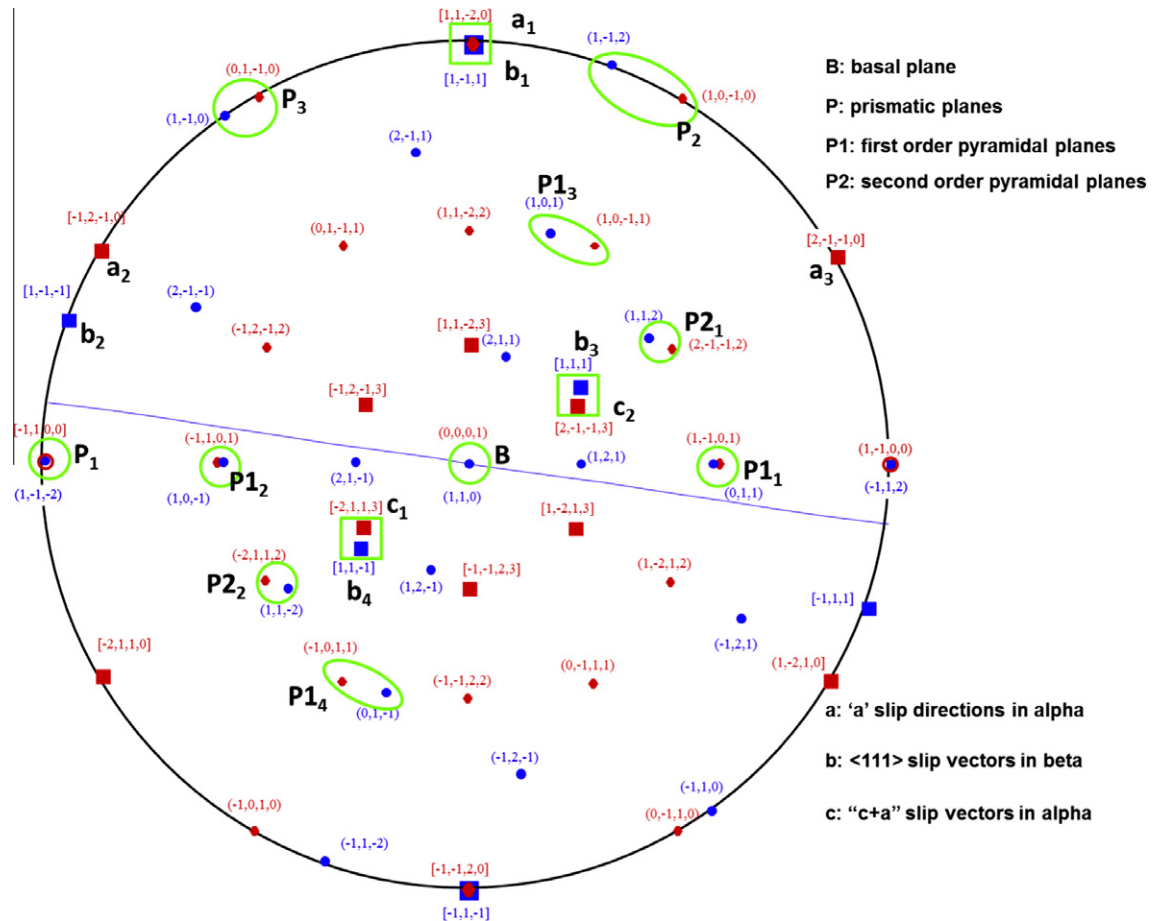


Fig. 33. Stereographic projection showing the alignment of slip planes and directions between the alpha and beta phases in a single variant of the alpha phase related to beta by the Burgers orientation. Green circles outline relatively close alignment. The macroscopic habit plane (blue trace) is shown.

structure is defined by a value of the ratio equal to 0.667. It has been observed that the stress-induced omega forms at room temperature when the omega phase has the ideal hexagonal structure. $\{3\bar{3}2\}\langle 113 \rangle$ twinning is preferred when the ratio decreases from this ideal value and finally slip is observed when this ratio decreases to below 0.662 (irrespective of the specific alloying content). Fig. 29c and d illustrates this effect with respect to temperature in the Ti–15V–3Al–3 Cr–3Sn alloy, a decrease in deformation temperature being equivalent to decreasing the beta stabilizer content in the sense that the beta phase becomes increasingly unstable and athermal omega is induced at liquid nitrogen temperatures in this alloy even though it is not present at room temperature.

The beta composition of conventionally heat-treated near alpha, alpha + beta or metastable beta alloys lies in the domain where slip is the preferred deformation mode of the beta phase. We note that slip can be quite planar in the beta phase as shown in Fig. 29c. Slip planarity can be intensified when clearly developed isothermal omega particles are present. The coherent omega precipitates are sheared during deformation, causing a decreasing resistance to continuing strain along the slip band, leading to

strain localization. Even when omega phase is not present, atomic displacements related to pre-omega or pre-martensitic instabilities act as in a manner equivalent to the presence of short-range order and promote the occurrence of planar slip in a similar manner. This is unusual for bcc metals and affects the work-hardening and strengthening behaviour of the beta phase.

4.3. The mechanical behaviour of alpha + beta titanium alloys

Most titanium alloys used in structural applications (of which Fig. 1b and c are examples) consist of two-phase mixtures of the alpha and beta phases combined in different morphologies and relative volume fractions, as illustrated in Fig. 13. Fig. 30 illustrates trends in key properties in these applications. The temperature capability of titanium alloys (Fig. 30a) is limited primarily by the oxidation and burn resistance of titanium, but also by the approach to beta transus (rather than the melting point of titanium), since the beta phase exhibits high diffusivity [1]. The range of properties sought in aeroengine applications, for example, is illustrated in Fig. 30b. This figure compares

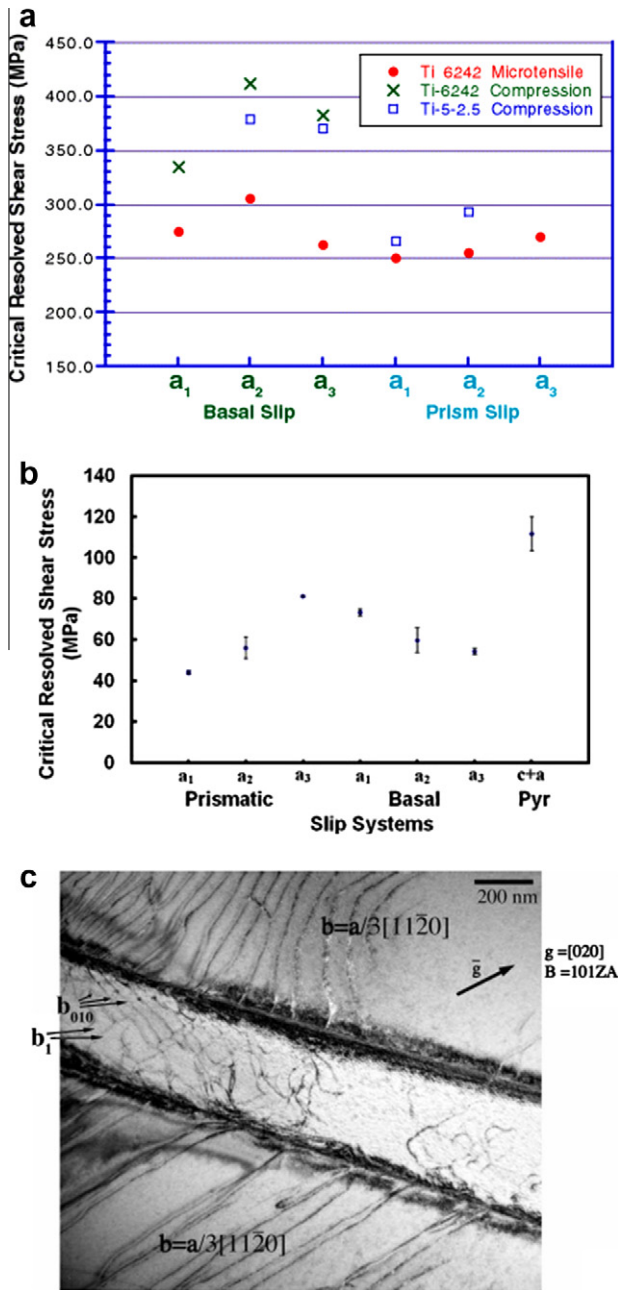


Fig. 34. (a) CRSS at room temperature of different slip systems in single colonies of alpha and beta phases [92]. (b) CRSS of different slip systems at 1078 K in a single colony of alpha and beta phases [93]. (c) Operation of the a_3 slip system in alpha showing $\langle 100 \rangle$ dislocations in beta [92].

the specific properties of IMI 834 (which has the highest temperature capability among conventional titanium alloys) with those of the workhorse Ni base superalloy IN718 at 923 K, and shows why titanium alloys give way to Ni-base alloys in applications requiring long term use at temperatures exceeding 873 K. Fig. 30c shows fracture-toughness yield strength combinations for titanium alloys. The superior combinations of strength and toughness that can be realized in the metastable beta alloys are evident and indicate why these alloys are preferred in airframe applications shown in Fig. 1c. These applications

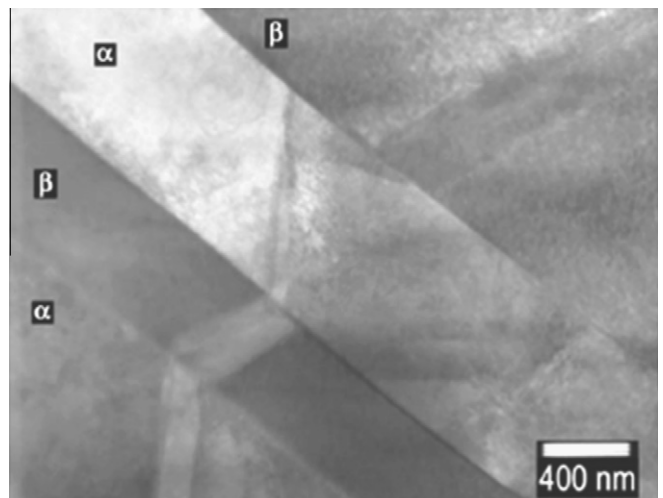


Fig. 35. Stress-induced martensite and twinning in alpha in response to tensile strain in Ti-8.1 V [94].

will continue to drive the improvement of this performance metric.

Qualitative relationships between microstructural features and properties of Ti alloys are well established and have been described in detail in Refs. [1,2] and will not be repeated here. Instead, we focus in this paper on more fundamental aspects of plasticity in these microstructures. Fig. 31 illustrates key microstructural parameters observed in a wide range of titanium alloys. Several microstructural length scales related to the alpha phase exist, ranging from very fine alpha laths in beta-enriched alloys to colonies of similarly oriented laths and to the equiaxed alpha phase morphology. The beta grain size (containing within these grains the transformed structure to alpha laths and retained beta) can vary quite significantly, ranging from several hundred microns in beta heat-treated near-alpha alloys to tens of microns in alpha + beta processed materials. The combinations of different length scales in the microstructure and the inability to vary each of these systematically independently of the other have led to an alternative analytical approach based on neural network analysis. This approach [89–91] extracts trends in mechanical behaviour as a function of different structural constituents from quantified microstructural features that are varied simultaneously. Fig. 32 shows examples of these trends in strength and toughness extracted from such analyses. Detailed crystal plasticity analysis is also being used to understand the mechanical response of two-phase alloys titanium alloys. Some of the more recent crystal plasticity based models are described in greater detail below.

4.3.1. The crystallography of slip and monotonic plasticity in two-phase structures

Structures that consist entirely of alpha laths having the Burgers relationship with the parent beta phase arise in different contexts: in beta-solution-treated materials

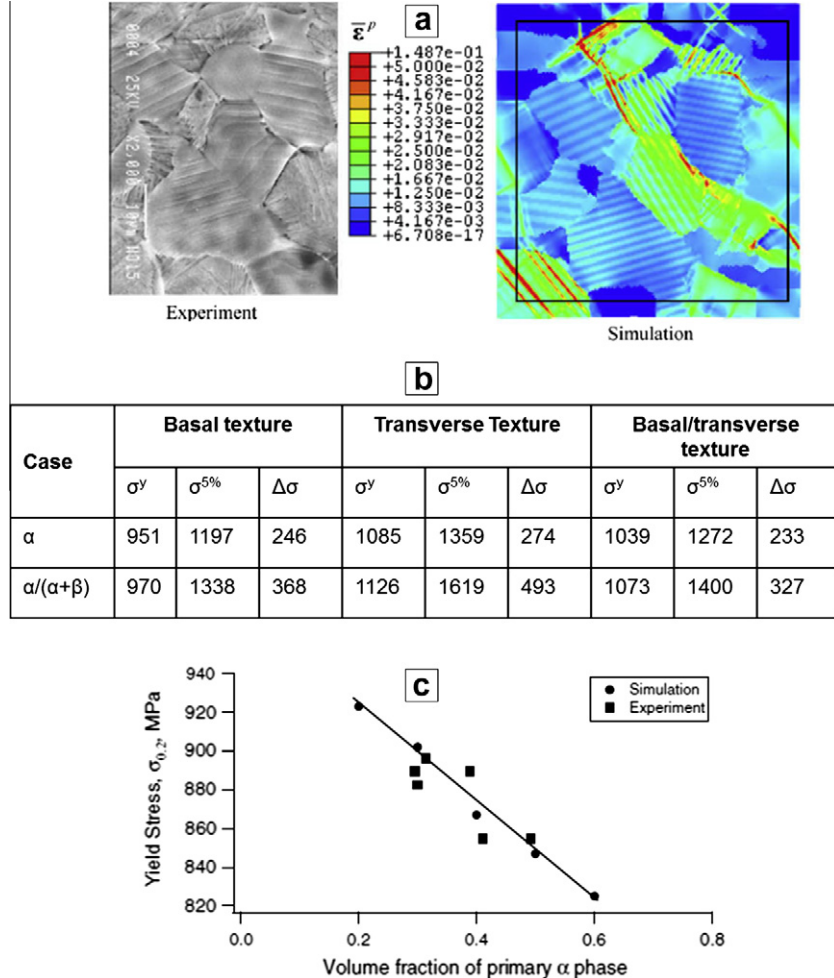


Fig. 36. (a) Slip in equiaxed alpha structures of Ti-64 modelled by crystal plasticity analysis [98]. (b) Prediction of flow stress in differently textured Ti-64 alloy [95]. (c) The prediction of yield stress with alpha volume fraction compared with experiment [96].

subsequently heat-treated in the alpha + beta region or as a constituent of microstructures that have been alpha + beta processed and heat-treated. The scale and distribution of these alpha laths can vary quite significantly, as shown in Fig. 7. Fig. 33 shows the relative orientations of common slip planes and slip directions in the alpha and beta phases related by the BOR. The basal slip plane of an alpha lath is parallel to a {110} slip plane of the beta phase. There are the three possible $\langle 11\bar{2}0 \rangle$ slip directions contained in the basal plane of the alpha phase. One labelled a_1 is almost precisely aligned with a $\langle 111 \rangle$ direction of beta, labelled b_1 . The other, labelled a_2 , lies at an angle of $\sim 11^\circ$ to the $\langle 111 \rangle$ direction labelled b_2 . The third (a_3) has no equivalent close packed beta slip direction in the basal plane. Of the three prismatic planes in alpha (marked P_1 , P_2 and P_3 in the figure), P_1 is precisely aligned to a {112} beta plane and this is also the plane that is nearly parallel to the habit plane and forms the terrace of the broad face of the interface between the two phases. In this case the corresponding slip directions a_1 and b_1 are aligned as well. We further note that first-order pyramidal planes P_{11} and P_{12} are nearly parallel to {110} planes of

the beta phase with a common slip direction in a_1 and b_1 . Two of the various possible second-order pyramidal slip planes, P_{21} and P_{22} are nearly parallel to {112} beta planes with nearly parallel $c+a$ (c_1 and c_2) and $\langle 111 \rangle$ beta slip directions. The ease of slip transfer will also depend on (a) the magnitude of Burgers vector change between the slip vectors of the two phases, which is $\sim 4\%$ between the close packed directions of the two phases and very large ($\sim 60\%$) between the $c+a$ and $\langle 111 \rangle$ direction; (b) the modulus differences between the two phases; (c) the mean free slip length in the phase within which slip initiates that will determine the local stress at the interface; (e) elastic differences between the two phases that will set up elastic interaction stresses at the interfaces that can affect the slip transfer process; and (f) the interaction of mobile dislocations with the geometrically necessary dislocations at the interface.

The critical resolved shear stress for various slip systems in a single colony of parallel-oriented alpha laths has been assessed both at room temperature [92] and at high temperatures [93], as shown in Fig. 34. While a single colony (Fig. 7a) effectively represents a single grain of the alpha

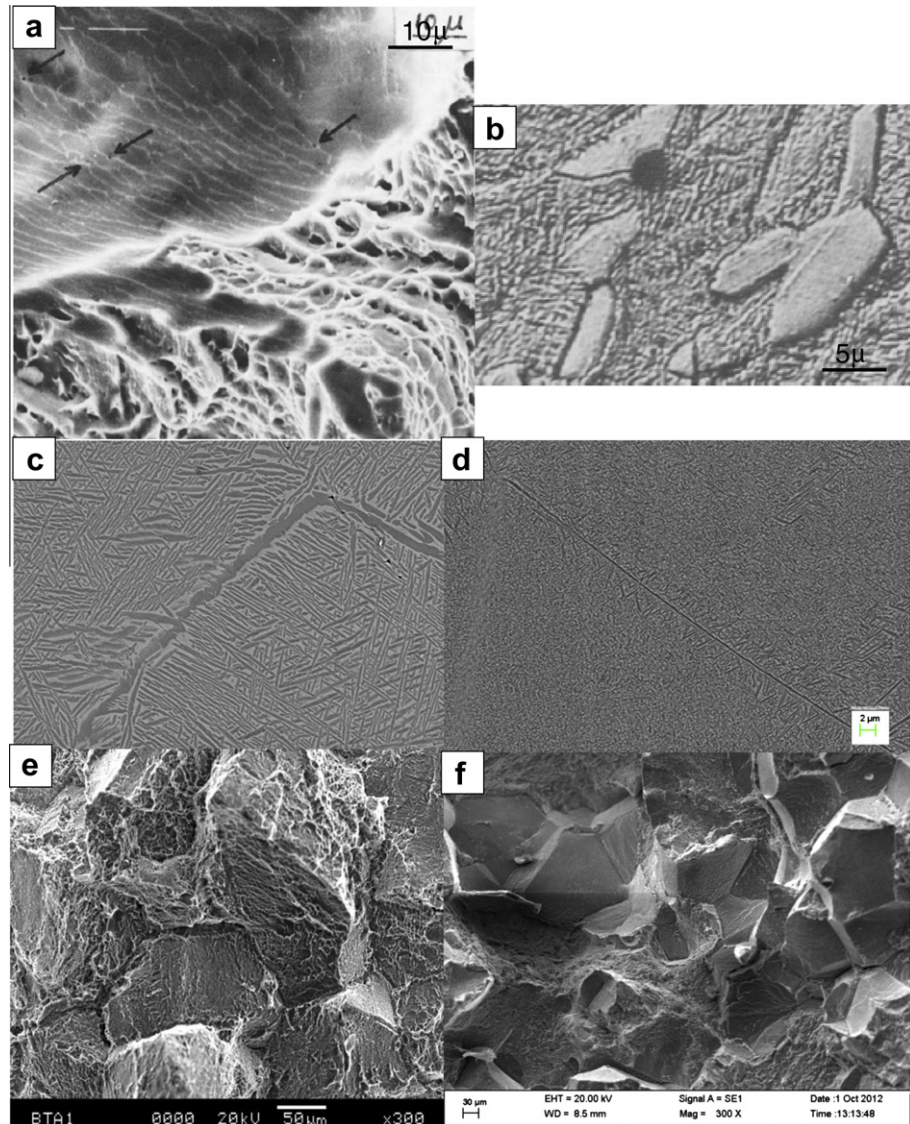


Fig. 37. (a) Void nucleation at alpha/beta interfaces of a colony structure in a beta heat-treated titanium alloy. The fracture surface and underlying microstructure are shown [130]. (b) Void nucleation at the interface of equiaxed alpha and transformed beta [131]. (c and d) Microstructures corresponding to the fractographs of (e) and (f) respectively after fracture toughness testing in a Ti-5553 alloy. (c) and (e) correspond to fracture toughness values of $80 \text{ MPa m}^{-1/2}$, while (d) and (f) correspond to fracture toughness values of $50 \text{ MPa m}^{-1/2}$ ((c–f) from Ref. [132]).

phase, equivalent slip systems of alpha are anisotropic because of differences in the ease of slip transfer across the thin regions of beta phase as discussed above. Somewhat surprisingly, the basal $[a_3]$ slip system does not have a significantly higher critical resolved shear stress in comparison with the basal $[a_1]$ and in some cases is actually lower in spite of the absence of an aligned $\langle 111 \rangle$ slip direction in the beta phase. However, slip bands on the basal plane are shown to initiate $\langle 100 \rangle$ slip in beta in this case [92] (Fig. 34c). There are no studies of slip transfer from pyramidal planes and the measured CRSS for pyramidal $\langle c+a \rangle$ slip at high temperature does not report which of the possible slip systems was excited [93]. Slip in these colony structures is initiated from the alpha phase since the plastically constrained thin regions of the beta phase are believed to be stronger. It is interesting to note

that the CRSS values do not differ significantly from those of single-phase alpha shown in Fig. 20.

However, microstructures dominated by large colonies of alpha laths rarely occur in application, except perhaps in castings and very thick section, beta-heat-treated products. Far more common are basket-weave structures or multivariant distributions of small colonies and individual plates seen in Fig. 13c–e. In these situations, the slip transfer processes (or the lack thereof) are significantly more complicated. With increasing volume fractions of the beta phase its larger, effective length scale reduces or eliminates the plastic constraint, and it is likely that this phase will become the softer of the two and initiate slip. Even in a multivariant distribution, closely aligned slip planes and directions do exist in many cases across the parent beta and different alpha variants. The discussion above refers

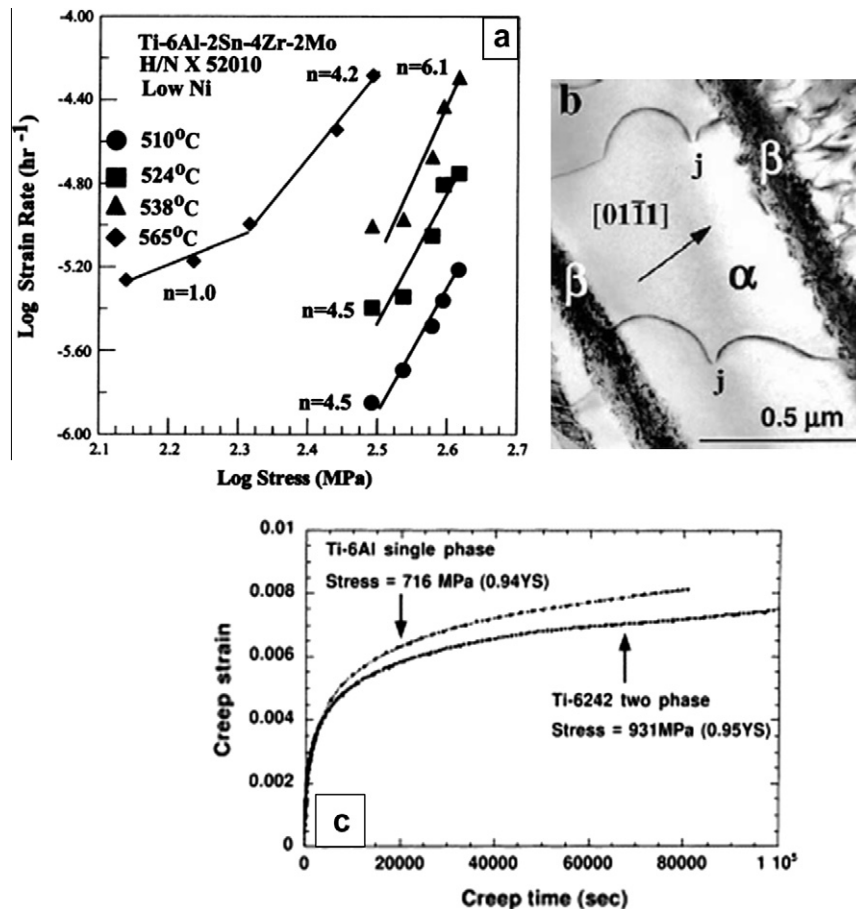


Fig. 38. (a) Stress exponents in steady state creep in a Ti-6242 alloy [102], (b) jogged screw dislocations in the alpha phase [103], (c) primary creep at room temperature [105].

to compositions where both the alpha and beta phases respond plastically by slip. In other cases, the alpha and beta phases may respond through the formation of stress-induced products [94] as shown in Fig. 35.

Bimodal structures containing equiaxed alpha and a transformed beta (lath alpha) constituent (Fig. 13) are used more often in application. In these microstructures, slip initiates in the equiaxed alpha [95–98] and slip behaviour is consistent with Schmid's law [97], at least on the surface. Finite element crystal plasticity models incorporating slip band softening as a consequence of destruction of short-range order as well as tension-compression asymmetry for prismatic planes (Section 4.1) and constant slip band spacing have been used to predict the intensity of slip within each equiaxed grain [97], as shown in Fig. 36. These models assume the transformed beta region to consist of a "homogenized" grain that represents single colonies of the lath structure with the same grain size as the lath structure. Easy slip modes (Section 4.3.1) in the colony are assumed to have a threshold stress that depends on the colony size while the threshold stress for hard slip modes are assumed to scale with the alpha lath size. "c" component slip has not been considered and the beta phase slip systems provide the

necessary plastic relaxation to accommodate strain along the "c" axis of the colonies. The yield stress is not significantly affected by the presence of the transformed beta constituent since plasticity is initiated in equiaxed alpha, but the flow stress at higher strains is significantly different when the transformed beta constituent is present [95].

Slip transfer into the transformed beta constituent is complex and has not been well modelled for reasons described earlier and also because detailed constitutive relations are not available in crystal plasticity models. Nevertheless, it is this class of microstructure that is utilized most often in titanium alloys with high combinations of strength and toughness (Figs. 1c, 13c and 30c).

4.3.2. A brief note on ductility and fracture

Ti and Ti alloys exhibit ductile fracture under normal loading except in a few special circumstances as when exposed to certain environments in the presence of a pre-existing crack. As mentioned earlier, Ti alloys do not contain hard, rigid and brittle second phases such as the carbides in steel and nickel-base alloys or the intermetallic constituent phases in high strength Al alloys. In these other classes of alloys ductile fracture is initiated either at the

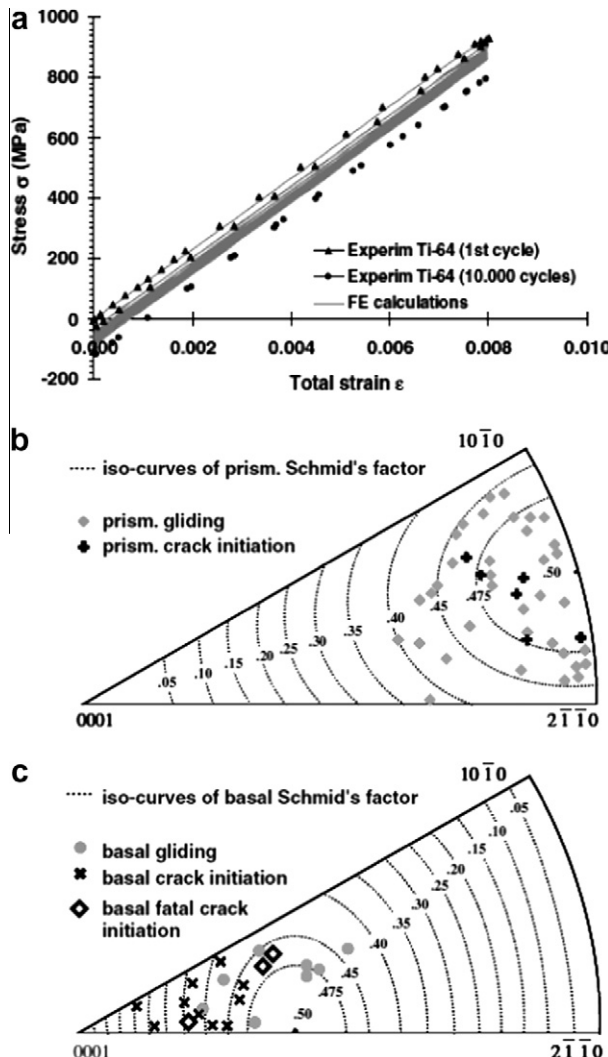


Fig. 39. (a) The prediction of cyclic stress-strain curves with crystal plasticity finite element modelling [107], (b) orientation of primary alpha grains with fatigue cracks in relation to the Schmid factor [108].

interface between the second phases and the metallic matrix, or at sharp cracks that form due to the fracture of the second phases and propagate by a ductile crack extension mode.

While improvements in the ductility and toughness of high strength steel and Al alloys derive from reducing the number of the crack initiation sites, the fracture of Ti alloys occurs by formation of microvoids at interphase interfaces or by shear related fracture of intensely planar and localized slip bands. Void nucleation occurs at sites of strain incompatibility in the former case. These are essentially the interfaces between grain boundary alpha and the matrix of transformed beta, or the interfaces between equiaxed alpha and the matrix of transformed beta, or if these constituents do not exist in the structure, the interfaces between lath, Burgers related alpha and beta (Fig. 37a and b show examples). The ease of void nucleation and growth will depend significantly on the

relative strengths of these constituents in the first two cases. Titanium alloys have a low work-hardening rate in general and this promotes easier void growth, resulting in ductile fracture at relatively low strains. Very low ductility intragranular fracture can occur for example if continuous grain boundary alpha is present along with fine, high strength transformed beta constituent (Fig. 37c and d). It is also clear that the crack path during fracture is heavily influenced by the spatial arrangement of these phases. Further, Ti alloys commonly exhibit an inverse correlation between tensile ductility and fracture toughness for a given microstructure. This apparent paradox is qualitatively explained if the preferred sites for microvoid nucleation and coalescence lead to crack paths with large tortuosity, as can happen when relatively soft grain boundary alpha is present. Very low ductility fractures can also arise from conditions that promote planar slip and severe strain localization. These include oxygen and aluminum contents beyond critical levels in the alpha phase, or heat treatments that promote short-range order in this phase in Al-containing alloys. The presence of high volume fractions of omega phase and extremely fine alpha dispersions in beta also promote slip localization in the beta phase.

The foregoing discussion suggests that the microstructure of Ti alloys can be tailored to result in either good ductility or high fracture toughness, but generally not both. Nevertheless, the ability to optimize the properties of Ti alloys for a particular design-limiting property is one of the factors that cause Ti alloys to be attractive for high performance structural applications.

4.3.3. Creep

The creep strength of titanium is influenced by several distinctive features. High temperature alloys maximize the volume fraction of alpha phase while incorporating adequate beta content for strength and refinement of microstructural scales as described earlier. It is well established that creep resistance decreases with equiaxed alpha volume fraction. Si in solid solution imparts creep resistance due to dynamic strain ageing while trace levels of Fe and Ni, impurities that arise from the titanium extraction process, are known to lower it. Finally, primary creep strains in titanium are quite high in relation to precipitation-hardened nickel-base alloys and lead to significant strain accumulation even at room temperature. Moreover, there is a high variability in the primary creep strain which is particularly troublesome when designing rotating parts with tight clearances between them and the static surroundings, as in aeroengines.

The high temperature, high stress creep of titanium shows stress exponents ranging from 4 and higher [99–102] and can be normalized to usual values for climb-controlled creep by the incorporation of a threshold stress [99,100]. The origin of the threshold stress is unclear but may be related to slip transfer processes across the two-phase interfaces. It is also possible that anomalous stress

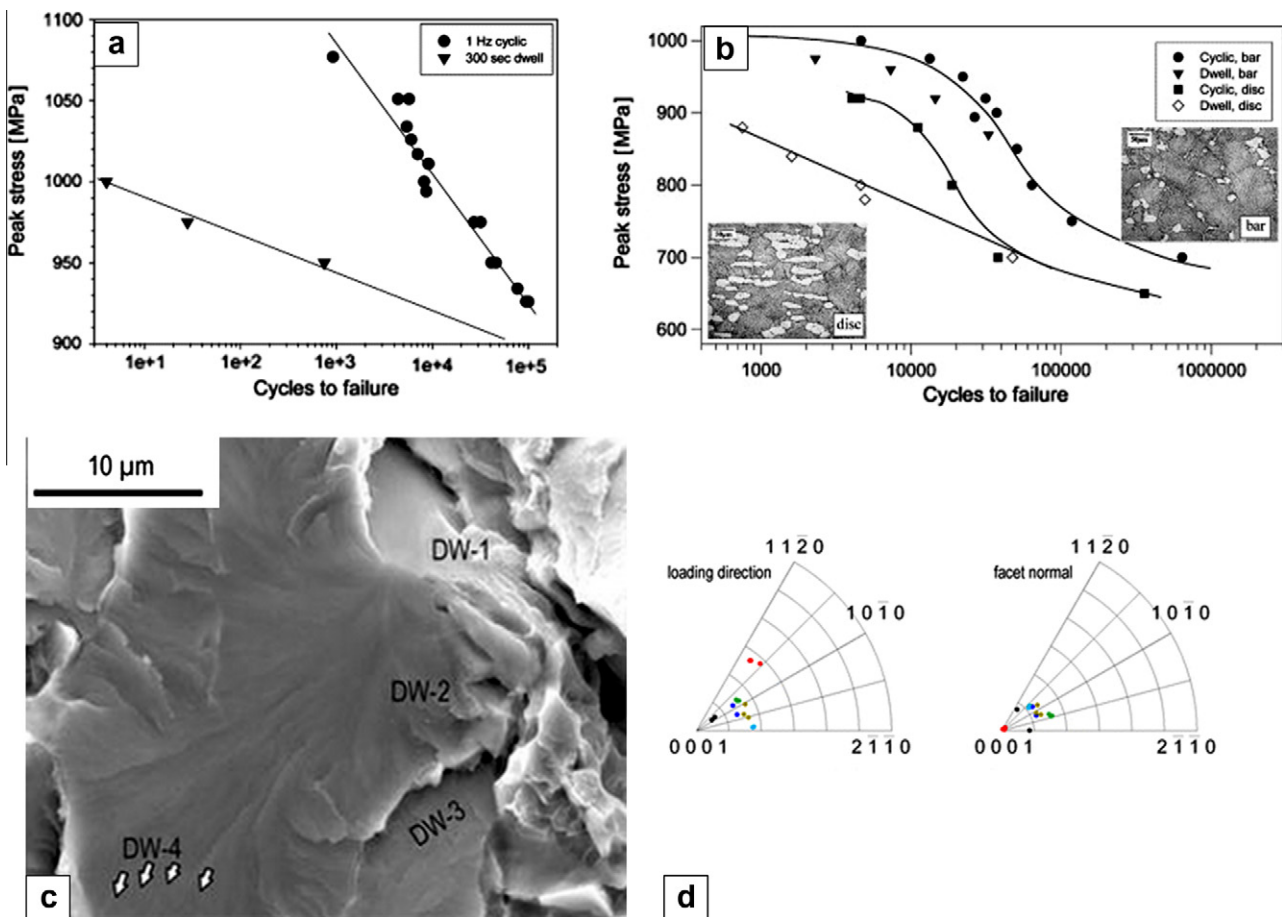


Fig. 40. The dwell effect on fatigue life [110] in (a) a beta heat-treated Ti-64 alloy with a colony structure and (b) laboratory samples and discs of duplex IMI834 alloy. (c) Crack initiation in dwell fatigue. DW-1 is parallel to a basal slip plane at $\sim 45^\circ$ to the stress axis while propagation facets DW2-4 lie at 8–26° from the loading direction and (d) cluster around an angle between 16° and 26° from the basal plane [118].

exponents arise from load transfer processes to the stronger alpha phase. It is also not understood why high values of stress exponents are obtained in some cases [99,100] and not in others [101,102]. Steady state creep is believed to be controlled by deformation processes in the alpha phase and a model based on the motion of jogged screw dislocations has been proposed [103] based on observations of tall jogs (Fig. 38). Importantly, this model incorporates an alpha length scale dependence on steady state creep rate through the effective screw dislocation line length on which jogs form. In alloy compositions without aluminium, the alpha and beta phases can respond in creep by twinning or by the formation of stress-induced products [94], and an unusual time-dependent response of twinning has recently been reported [104].

A transition to stress exponents of 1 at low stress levels and high temperatures has also been recorded and attributed to Harper Dorn creep [103]. Alpha/beta and alpha/alpha interface sliding has often been reported as contributing to creep strains [1,94,100] and it is quite possible that a part of the lower creep resistance of equiaxed structure and very fine lath structures [100] arises from an interface sliding contribution.

Fig. 38 also shows the small but finite primary strain that can accumulate at room temperatures in titanium alloys in both single-phase alpha and an alpha + beta alloy. The creep mechanism is exhaustive in nature. It has been suggested [105] that this behaviour arises from a significantly lower strain-hardening exponent in Ti at similar levels of strain rate sensitivity as in other metals. It has also been shown that heat treatment to manipulate short-range order affects primary creep rates at room temperature [106]. This phenomenon plays a central role in changing the fatigue behaviour of these alloys if the load is held at maximum value for as much as 2 min as opposed to continuously cycling. In near alpha titanium alloys such as Ti-6242, reductions in fatigue life that exceed a factor of 10 are commonly observed under conditions of dwell loading.

4.3.4. Fatigue

Crystal plasticity models of high cycle fatigue of duplex structures have been attempted recently [95,107,108]. The assumptions in these models have been described earlier for monotonic loading. In addition, evolving back stresses are described through an Armstrong–Frederick relation

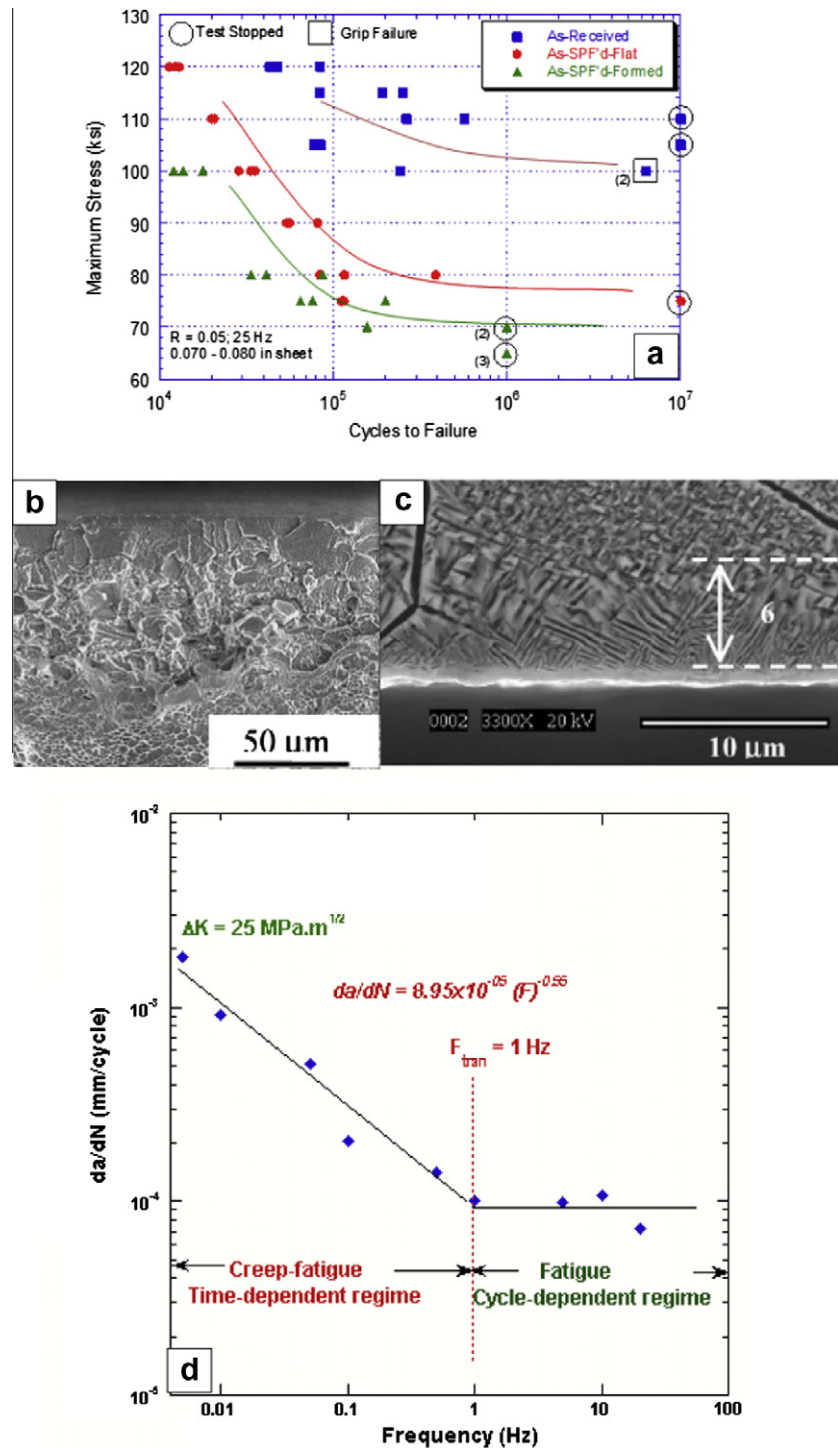


Fig. 41. (a) The effect of exposure at high temperatures (resulting in alpha case formation) during superplastic forming to flat and formed shapes on fatigue resistance of Ti-64 sheet [120]. (b) Tensile fracture surface of Ti-15Mo-2.7Nb-3Al-0.2 Si (Timetal-21S) after exposure at 923 K for 118 h [133]. (c) The modification of surface structure of the same alloy sheet after exposure at 923 K for 80 h [133]. (d) The effect of cyclic frequency on fatigue crack growth rate in the Paris regime in the IMI834 alloy tested at 873 K (courtesy Vikas Kumar).

and softening is assumed to occur for the first activated slip system in any grain to mimic direct observations of single slip at small strains. Fig. 39a shows the agreement of predicted cyclic strains with experimental data. Slip occurs

only on basal and prismatic planes with very low levels of multiple slip, and primarily in the equiaxed alpha grains at these low strain levels. Crack nucleation has been observed on both basal and prismatic planes in primary alpha grain

orientations with high Schmid factors for these slip systems (Fig. 39b). Nevertheless, it is the basal cracks that form the fatal cracks in this study and it is suggested that the coupling of single slip with hard elastic conditions favours basal crack initiation and growth as well as the observed crack orientations towards the basal pole away from the high Schmid factor orientations.

The fatigue behaviour of titanium represents an unusual phenomenon in that there is the strong ambient temperature dwell fatigue effect mentioned earlier which can significantly reduce fatigue life. Fig. 40 shows this in two different alloys, one that has been beta heat-treated and the other alpha+beta heat treated. This effect first manifested itself through the uncontained failure of aeroengine discs in the 1970s. Bache [109] in 2003 reviewed the phenomenon and its attribution to load transfer to hard alpha orientations (with their “c” axis parallel to the stress axis) due to the effect of slip bands impinging upon these orientations from surrounding soft grains in a Stroh type of model [110]. Failure occurred due to strongly faceted crack nucleation in the hard grains at subsurface sites. It was recognized that the kinetics of the process (the dwell effect) could arise from the ambient and low temperature creep strain accumulation described earlier. It was also recognized that the presence of macrozones of preferred orientations in duplex structures discussed in Section 3 or lath colonies with aligned alpha structures promoted early failure. The kinetics of the load shedding process as a consequence of creep relaxation of soft grains surrounding hard orientations during the ambient temperature dwell has been explored both in polycrystalline single-phase alpha and duplex Ti6242 alloy through crystal plasticity analysis [111–113]. The analysis also suggested that the grain size of the soft grains surrounding the hard would influence the load-shedding process and not vice versa. More recently, the load-shedding phenomenon has been coupled to crack nucleation criterion in the hard grain based on dislocation pile-up induced wedge crack formation at the soft/hard grain boundary [114–116]. However, careful analysis of faceted fatigue nucleation sites in cyclic fatigue with and without dwell exhibit interesting differences in crack crystallography [117,118]. Dwell fatigue fracture initiation facets are shown [118] to initiate at the intersection between primary alpha grains with the basal plane lying close to the maximum shear stress plane and a grain in a hard orientation (Fig. 40c and d). Thus, the initiation site contains a smooth facet which lies along the basal slip plane in a suitably oriented grain of the alpha phase. Curiously, these immediately transition to facets parallel to near basal planes lying nominally perpendicular to the loading axis in surrounding hard orientations. In contrast, cyclic loads without dwell result in surface initiation on basal slip planes that lie within 25° to 45° of the stress axis and propagate along these planes. It has also been reported recently that dwell effects can occur in samples that contain no hard orientations either of the alpha phase or in aligned colonies [119]. The balance of evidence

suggests that the role of hydrogen in dwell fatigue fracture, while not explicitly incorporated at this time, cannot be discounted.

4.3.5. High temperature exposure and mechanical behaviour

While room temperature dwell time effects on fatigue behaviour on titanium are unique, the high solubility of oxygen in titanium affects the properties of titanium alloys at high temperatures and can limit the temperature capability of titanium alloys that experience long term thermal exposure in application. In these environments, the surfaces of titanium alloys are modified progressively by changes in the volume fraction of the alpha phase until a single-phase alpha layer (called an alpha casing) on the surface results. Further exposure results in the formation of oxide. This surface layer can be brittle even when oxide is not present because oxygen in solid solution beyond controlled levels hardens and embrittles the alpha phase of titanium into which it partitions (Fig. 2). Fig. 41a shows, as an example, the effect of thermal exposure during superplastic forming of a sheet titanium alloy. Beta-rich alloys are affected (Fig. 41b and c) as well, as shown by brittle crack initiation from the surface of a thermally exposed sample in a tensile test. In addition to the unusual room temperature dwell effects on fatigue life that have been discussed earlier, conventional creep–environment–fatigue interaction effects are observed as well at high temperatures. Fig. 41d illustrates this effect in the form of a cycle frequency dependence of fatigue crack growth at low cycle frequencies.

5. Summary

In the past ~20 years, Ti alloys have become increasingly important structural materials for high-value, weight-sensitive products. The successes of applying Ti alloys have largely been the result of pragmatic engineering as opposed to bottom-up scientific discovery and application. Nevertheless, Ti alloys are being successfully used in aircraft, aircraft engines and rocket engines, among other products. As product realization cycles become shorter, the benefit of using modelling and simulation to reduce the time and cost of qualifying materials for a given application becomes increasingly important. High-fidelity models require sound physical understanding of the phenomena that govern materials behaviour. To this end we have attempted to identify areas where additional research can enable better models.

Titanium alloys derive their properties from combinations of the two ductile phases based the hcp and bcc allotropic modifications of titanium. Several key features of these phases individually and in combination determine the plasticity and fracture behaviour of these single-phase or two-phase mixtures. The alpha phase is both elastically and plastically anisotropic and stiffer and stronger when oriented with its c-axis parallel to the loading direction. Thus texture, both global and local, plays a key role in

its plasticity. Its anisotropy extends to dislocation behaviour through the non-planar core spread of screw “a” type dislocations that render this line direction relatively immobile. Composition, especially the Al and O content of alpha, sensitively affects its plasticity through its twinning response and slip character, whether planar or homogeneous, through short-range order effects. The fundamental role of alloying additions on plasticity at the atomistic level remains poorly understood. It is also possible that hydrogen at relatively low concentration levels plays larger role in determining ambient-temperature time-dependent properties than has been recognized thus far. Creep properties of the alpha phase are better than those of beta because of the intrinsically lower diffusivities in its close packed structure. Nevertheless the alpha phase can accumulate relatively large plastic strains at ambient temperatures under constant loading conditions below its yield stress. A strong interaction of dynamic strain ageing phenomena in the alpha phase with the creep process exists at intermediate temperatures but has not been well documented thus far.

The beta phase has a variable modulus and its elastic behaviour including anisotropy can be controlled through alloying additions. It is also subject to a variety of thermal and stress-induced phonon and shear instabilities, a detailed understanding of which is only now beginning to emerge as the biomedical community exploits its low toxicity combined with a bone-matched modulus, in both conventional and shape-memory-related applications.

In combination, the alpha and beta phases can be crystallographically oriented in a manner that strongly affects the plasticity of the two-phase mixture by enhancing anisotropy of slip through preferential alignment of some slip planes and directions in the two phases. Thermomechanical processing is used to relatively reorient and obtain more isotropic morphologies of the two phases. Quite recently, however, it has emerged that under many conventional processing conditions, especially in thick section products, microtextures reflecting this strong crystallographic alignment continue to persist and affect properties in unusual ways. Therefore, efforts to understand and model thermal and compositional effects on crystallographic variant distribution of the alpha phase as it precipitates from the parent beta, and the effects of variant selection on the pathways of subsequent microstructural evolution during processing, have only just begun to emerge.

Acknowledgements

One of the authors (DB) is grateful for the support of the Department of Materials Engineering, University of North Texas, and in particular Rajarshi Banerjee, during a substantial part of the writing of this paper.

References

- [1] Lutjering G, Williams JC. Titanium. 2nd ed. Berlin: Springer; 2007.
- [2] Leyens C, Peters M. Titanium and titanium alloys. Weinheim: Wiley-VCH; 2003.
- [3] Banerjee S, Mukhopadhyay P. Phase transformations, examples from titanium and zirconium alloys. Oxford: Elsevier; 2007.
- [4] Saunders N. In: Bleckinsop P, Evans WJ, Flower HM, editors. Titanium '95: science and technology. London: Institute of Materials; 1996. p. 2167.
- [5] Glavicic MG, Kobryn PA, Spadafora F, Semiatin SL. Mater Sci Eng A 2003;346:8.
- [6] Kalinyuk AN, Trigub NP, Zamkov VN, Ivasishin OM, Markovsky PE, Teliovich PE, et al. Mater Sci Eng A 2003;346:178.
- [7] Roy S, Suwas S, Tamirisakandala S, Miracle DB, Srinivasan R. Acta Mater 2011;59:5494.
- [8] Furuhara T, Howe JM, Aaronson HI. Acta Metall Mater 1991;39: 2873.
- [9] Pilchak A, Banerjee D, Williams JC. Unpublished research. Ohio State University; 2009.
- [10] Settefrati A, Appolaire B, Aeby-Gautier E, Le Bouar Y, Khelifati G. In: Zhou L, Chang H, Lu Y, Xu D, editors. Ti-2011. Beijing: National Science Press; 2012. p. 474.
- [11] Shi R, Ma N, Wang Y. Acta Mater 2012;60:4172.
- [12] Furuhara T, Takagi S, Watanabe H, Maki T. Metall Mater Trans A 1996;27:1635.
- [13] Bhattacharyya D, Viswanathan GB, Fraser HL. Acta Mater 2007;55:6765.
- [14] Nag S, Banerjee R, Srinivasan R, Hwang JY, Harper M, Fraser HL. Acta Mater 2009;57:2136.
- [15] Aeby-Gautier E, Settefrati A, Bruneseaux F, Appolaire B, Denanda B, Dehmasa M, et al. J Alloy Compd, in press. <http://dx.doi.org/10.1016/j.jallcom.2012.02.046>.
- [16] Vanderesse N, Maire E, Darrieulat M, Montheillet F, Moreaud M, Jeulin D. Scripta Mater 2008;58:512.
- [17] Sharma H, van Bohemen SMC, Petrov RH, Sietsma J. Acta Mater 2010;58:2399.
- [18] Banumathy S, Mandal RK, Singh AK. J Appl Phys 2009;106: 093518.
- [19] Banerjee D, Muraleedharan K, Strudel JL. Philos Mag A 1998;77: 299.
- [20] Tahara M, Young Kim H, Inamura T, Hosoda H, Miyazaki S. Acta Mater 2011;59:6208.
- [21] Yano T, Murakami Y, Shindo D, Kuramoto S. Acta Mater 2009;57: 628.
- [22] Otsuka K, Wayman CM, Kubo H. Metall Trans A 1978;9:1075.
- [23] Hanada S, Izumi O. Metall Trans A 1986;17:1409.
- [24] Nag S, Devaraj A, Srinivasan R, Williams REA, Gupta N, Viswanathan GB, et al. Phys Rev Lett 2011;106:24570.
- [25] Harmon EL, Troiano AR. Trans ASM 1961;53:43.
- [26] Hari Narayanan G, Luhman TS, Archbold TF, Taggart R, Polonis DH. Metallography 1971;4:343.
- [27] Koul MK, Breedis JF. Acta Metall 1970;18:579.
- [28] Afonso CRM, Ferrandini PL, Ramirez AJ, Caram R. Acta Biomater 2010;6:1625.
- [29] Devaraj A, Nag S, Srinivasan R, Williams REA, Banerjee S, Banerjee R, Fraser HL. Acta Mater 2012;60:596.
- [30] Mohamed Abdel-Hady, Hinoshita K, Morinaga M. Scripta Mater 2006;55:477.
- [31] Inamura T, Hosoda H, Young Kim H, Miyazaki S. Philos Mag 2010;90:3475.
- [32] Semiatin SL, Seetharaman V, Weiss I. JOM 1997;49(6):33.
- [33] Weiss I, Semiatin SL. Mater Sci Eng A 1998;243:46.
- [34] Weiss I, Semiatin SL. Mater Sci Eng A 1999;263:243.
- [35] Banerjee D, Pilchak AL, Williams JC. Mater Sci Forum 2012;710: 66.
- [36] Singh AK, Schwarzer RA. Trans Ind Inst Metal 2008;61:371.

- [37] Lonardelli I, Gey N, Wenk H-R, Humbert M, Vogel SC, Lutterotti L. *Acta Mater* 2007;55:5718.
- [38] Mironov S, Murzinova M, Zherebtsov S, Salishchev GA, Semiatin SL. *Acta Mater* 2009;57:2470.
- [39] Margolin H, Cohen P. In: Kimura H, Izumi O, editors. Titanium 80, science and technology. Warrendale, PA: TMS; 1980. p. 1555.
- [40] Weiss I, Welsch GE, Froes FH, Eylon D. In: Lutjering G, Zwicker U, Bunk W, editors. Titanium: science and technology. Oberursel: Deutsche Gesellschaft für Metallkunde; 1985. p. 1503.
- [41] Semiatin SL, Seetharaman V, Ghosh AK. *Phil Trans Roy Soc Lond A* 1999;357:1487.
- [42] Semiatin SL, Bieler TR. *Acta Mater* 2001;49:3565.
- [43] Bieler TR, Semiatin SL. *Int J Plasticity* 2002;18:1165.
- [44] Gey N, Bocher P, Uta E, Germain L, Humber M. *Acta Mater* 2012;60:2647.
- [45] Cayron C. *Scripta Mater* 2008;59:570.
- [46] Ogi H, Kai S, Ledbetter H, Tarumi R, Hirao M, Takashima K. *Acta Mater* 2004;52:2075.
- [47] Hao YanJun, Zhu Jun, Zhang Lin, Qu JianYing, Ren HaiSheng. *Solid State Sci* 2010;12:1473.
- [48] Tanaka T, Conrad H. *Acta Metall* 1972;20:1019.
- [49] Williams JC, Baggerly RG, Paton NE. *Metall Mater Trans A* 2002;33:837.
- [50] Naka S, Lasalmonie A, Costa P, Kubin LP. *Philos Mag A* 1988;57:717.
- [51] Farenc S, Caillard D, Couret A. *Acta Metall Mater* 1995;43:3669.
- [52] Ghazisaeidi M, Trinkle DR. *Acta Mater* 2012;60:1287.
- [53] Gong J, Wilkinson AJ. *Acta Mater* 2009;57:5693.
- [54] Salem AA, Kalidindi SR, Doherty RD. *Scripta Mater* 2002;46:419.
- [55] Salem AA, Kalidindi SR, Doherty RD. *Acta Mater* 2003;51:4225.
- [56] Salem AA, Kalidindi SR, Doherty RD, Semiatin SL. *Metall Mater Trans A* 2006;37:259.
- [57] Chun YB, Yu SB, Semiatin SL, Hwang SK. *Mater Sci Eng A* 2005;398: 209.
- [58] Conrad H. *Prog Mater Sci* 1981;26:123.
- [59] Fleischer RL. *Scripta Metall* 1987;21:1083.
- [60] Senkov ON, Jonas JJ. *Metall Mater Trans A* 1996;27:1877.
- [61] Prasad K, Kamat SV. *Mater Sci Eng A* 2008;490:477.
- [62] Paton NE, Williams JC, Rauscher GP. Titanium science and technology, vol. 2. New York: Plenum. 1973. p. 1049.
- [63] Williams JC, Tung PP, Sommer AW. *Metall Trans* 1972;3:2979.
- [64] Churchman A. *Proc Roy Soc A* 1954;226:216.
- [65] Brandes M, Baughman, Mills MJ, Williams JC. *Mater Sci Eng A* 2012;551:13.
- [66] Nixon ME, Cazacu O, Lebensohn RA. *Int J Plasticity* 2010;26:516.
- [67] Salem AA, Kalidindi SR, Semiatin SL. *Acta Mater* 2005;53:3495.
- [68] Bradley S, Fromm BS, Adams BL, Ahmadi S, Knezevic M. *Acta Mater* 2009;57:2339.
- [69] Wang L, Barabash RI, Yang Y, Bieler TR, Crimp MA, Eisenlohr P, et al. *Metall Mater Trans A* 2011;42:626.
- [70] Yang Y, Wang L, Bieler TR, Eisenlohr P, Crimp MA. *Metall Mater Trans A* 2011;42:636.
- [71] Alankar A, Eisenlohr P, Raabe D. *Acta Mater* 2011;59:7003.
- [72] Biesiekierski A, Wang J, Mohamed Abdel-Hady Gepreel, Wena C. *Acta Biomater* 2012;8:1661.
- [73] Geetha M, Singh AK, Asokamani R, Gogia AK. *Prog Mater Sci* 2009;54:397.
- [74] Tane M, Akita S, Nakano T, Hagihara K, Umakoshi Y, Niinomi M, et al. *Acta Mater* 2010;58:6790.
- [75] Tane M, Nakano T, Kuramoto S, Hara M, Niinomi M, Takesue N, et al. *Acta Mater* 2011;59:6975.
- [76] Zhang YW, Li SW, Obbard EG, Wang H, Wang SC, Hao YL, et al. *Acta Mater* 2011;59:3081.
- [77] Lee S-H, Todai M, Tane M, Hagihara K, Nakajima H, Nakano T. *J Mech Behavior Biomed Mater* 2012;14:48.
- [78] Hermann R, Hermann H, Calin M, Buchnera BJ, Eckert J. *Scripta Mater* 2012;66:198.
- [79] Zhang DC, Lin JG, Jiang WJ, Ma M, Peng ZG. *Mater Des* 2011;32:4614.
- [80] Taharaa M, Kima HY, Hosoda H, Name T-H, Miyazaki S. *Mater Sci Eng A* 2010;527:6844.
- [81] Buenconsejo PJS, Kim HY, Hosoda H, Miyazaki S. *Acta Mater* 2009;57:1068.
- [82] Saito T, Furuta T, Hwang J-H, Kuramoto S, Nishino K, Suzuki N, et al. *Science* 2003;300:464.
- [83] Gutkin M Yu, Ishizaki T, Kuramoto S, Ovid'ko IA, Skiba NV. *Int J Plasticity* 2008;24:1333.
- [84] Obbard EG, Hao YL, Talling RJ, Li SJ, Zhang YW, Dye D, et al. *Acta Mater* 2011;59:112.
- [85] Bhattacharjee A, Varma VK, Kamat SV, Gogia AK, Bhargava S. *Metall Mater Trans A* 2006;37:1424.
- [86] Hanada S, Izumi O. *Metall Trans A* 1980;11:1447.
- [87] Hanada S, Ozeki M, Izumi O. *Metall Trans* 1985;16:789.
- [88] Hanada S, Izumi O. *Metall Trans A* 1987;18:265.
- [89] Kar S, Searles T, Lee E, Viswanathan GB, Tiley J, Banerjee R, Fraser HL. *Metall Mater Trans A* 2006;37:559.
- [90] Peterson B, Collins P, Fraser HL. *Mater Sci Eng A* 2009;513–514:357.
- [91] Collins PC, Koduri S, Dixit SV, Fraser HL, submitted for publication.
- [92] Savage MF, Tatalovich J, Mills MJ. *Philos Mag* 2004;84:1127.
- [93] Salem AA, Semiatin SL. *Mater Sci Eng A* 2009;508:114.
- [94] Ankem S, Margolin H, Greene CA, Neuberger BW, Oberson PG. *Prog Mater Sci* 2006;51:632.
- [95] Mayeur JR, McDowell DL. *Int J Plasticity* 2007;23:1457.
- [96] Zhang M, Zhang J, McDowell DL. *Int J Plasticity* 2007;23:1328.
- [97] Bridier F, Villechaise P, Mendez J. *Acta Mater* 2005;53:555.
- [98] Zhang M, Bridier F, Villechaise P, Mendez J, McDowell DL. *Acta Mater* 2010;58:1087.
- [99] Evans WJ, Harrison GF. *J Mater Sci* 1983;18:3449.
- [100] Mukherjee D, Banerjee D, Muraleedharan K. *Trans Ind Inst Metal* 1989;42:S185.
- [101] Es-Souni M. *Metall Mater Trans A* 2001;32:285.
- [102] Hayes RW, Viswanathan GB, Mills MJ. *Acta Mater* 2002;50:4953.
- [103] Viswanathan GB, Karthikeyan S, Hayes RW, Mills MJ. *Acta Mater* 2002;50:4965.
- [104] Oberson PG, Ankem S. *Phys Rev Lett* 2005;95:165501.
- [105] Neeraj T, Hou D-H, Daehn GS, Mills MJ. *Acta Mater* 2000;48:1225.
- [106] Neeraj T, Mills MJ. *Mater Sci Eng A* 2001;319–321:415.
- [107] Bridier F, McDowell DL, Villechaise P, Mendez J. *Int J Plasticity* 2009;25:1066.
- [108] Bridier F, Villechaise P, Mendez J. *Acta Mater* 2008;56:3951.
- [109] Bache MR. *Int J Fatigue* 2003;25:1079.
- [110] Evans WJ, Bache MR. *Int J Fatigue* 1994;16:443.
- [111] Sinha V, Spowart JE, Mills MJ, Williams JC. *Metall Mater Trans A* 2006;37:1507.
- [112] Hasija V, Ghosh S, Mills MJ, Joseph DS. *Acta Mater* 2003;51:4533.
- [113] Venkatramani G, Ghosh S, Mills MJ. *Acta Mater* 2007;55:3971.
- [114] Kirane K, Ghosh S. *Int J Fatigue* 2008;30:2127.
- [115] Kirane K, Ghosh S, Groeber M, Bhattacharjee A. *J Eng Mater Tech ASME* 2009;131(27):37.
- [116] Anahid M, Samal MK, Ghosh S. *J Mech Phys Solids* 2011;59:2157.
- [117] Sinha V, Mills MJ, Williams JC. *Metall Mater Trans A* 2004;35:3141.
- [118] Pilchak AL, Williams JC. *Metall Mater Trans A* 2011;42:1000.
- [119] Sackett EE, Germain L, Bache MR. *Int J Fatigue* 2007;29:2015.
- [120] Cotton JD, Boyer R. Personal communication. Seattle (WA): The Boeing Company; 2012.
- [121] Bermingham MJ, McDonald SD, Buddery AJ, StJohn DH, Dargusch MS. *Mater Sci Eng C* 2011;31:1520.
- [122] Roy S. PhD thesis. Indian Institute of Science; 2012.
- [123] Banerjee D, Hall JA, Williams JC. Unpublished research. Carnegie Mellon University; 1984.

- [124] Srinivasan R, Banerjee R, Viswanathan GB, Nag S, Hwang JY, Tiley J, et al. JOM 2010;62(12):64.
- [125] Shanoob B, Samajhdar I, Suwas S, Banerjee D. Unpublished research. Indian Institute of Science; 2012.
- [126] Sajid Hussain. ME thesis. Indian Institute of Science; 2011.
- [127] Banerjee D, Williams JC. Unpublished research. Ohio State University; 2008.
- [128] Banerjee D, Okada M, Williams JC. Unpublished research. Carnegie Mellon University; 1984.
- [129] Hertzberg A, Rosenfield AR, McEvily Jr. AJ, NATO AGARD Report 610; 1973. p. 23.
- [130] Banerjee D, Mukherjee D, Saha RL, Bose K. Metall Trans A 1983;14:413.
- [131] Greenfield MA, Margolin H. Metall Trans 1972;3:2649.
- [132] Ghosh A, Shivaprasad S, Kar S, Bhattacharjee A, Banerjee D. Unpublished research. India: IIT Kharagpur; 2012.
- [133] Sansoz F, Almesallmy M, Ghonem H. Metall Mater Trans A 2004;35:3115.